Quaternary Science Reviews 29 (2010) 1382–1398

Contents lists available at ScienceDirect

Quaternary Science Reviews

journal homepage: www.elsevier.com/locate/quascirev

Middle and Late Pleistocene paleoscape modeling along the southern coast of South Africa

Erich C. Fisher [a,*], Miryam Bar-Matthews [b], Antonieta Jerardino [c], Curtis W. Marean [d]

[a] Department of Anthropology, University of Florida, Gainesville, FL 32611-7305, USA
[b] Geological Survey of Israel, 30 Malchei Israel Street, Jerusalem 95501, Israel
[c] Catalan Institute for Research and Advanced Studies (ICREA)/GEPEG, Department of Prehistory, Ancient History and ArchaeologyArcheology, University of Barcelona, c/Montalegre, 6-8, E-08001 Barcelona, Spain
[d] Institute of Human Origins, School of Human Evolution and Social Change, Arizona State University, Tempe, AZ 85287-2402, USA

ARTICLE INFO

Article history:
Received 26 August 2009
Received in revised form
26 January 2010
Accepted 27 January 2010

ABSTRACT

Changing climates, environment, and sea levels during the Middle and Late Pleistocene must have had significant impacts on early modern humans and their behavior. However, many important archaeological sites occur along the current coastline of South Africa where the gradual slope of the offshore Agulhas Bank meant that small changes to sea level height potentially caused significant shifts in coastline position. The geographic context of these currently coastal sites would have been transformed by sea level shifts from coastal to near-coastal to fully terrestrial. To understand human adaptations as reflected in the archaeological deposits of these now-coastal sites we need to accurately model coastline position through time. Here, we introduce a Paleoscape model as a conceptual tool to ground the records for human behavioral evolution within a dynamic model of paleoenvironmental changes. Using integrated bathymetric datasets, GIS, and a relative sea level curve we estimate the position of the coastline at 1.5 ka increments over the last ~420,000 years. We compare these model predictions to strontium isotope ratios from speleothems as an independent test and then compare the coastline predictions to evidence for shellfish exploitation through time. Both tests suggest our model is relatively robust. We then widen our paleoscape model to most of the Cape region and compare the predictions of this broadened model to evidence from Blombos cave.

1. Introduction

Sea caves around the world often contain rich archaeological records of human occupation. Along the south coast of South Africa this is well illustrated by a set of caves (e.g. Die Kelders Cave 1, Blombos, Pinnacle Point 13B, Nelson Bay Cave, and Klasies River) that contain sedimentary and archaeological sequences that span the late Middle Pleistocene to the Holocene (Fig. 1). These sequences have figured prominently in our understanding of the evolution of modern humans (Grine, 1998; Henshilwood et al., 2002, 2004; Marean et al., 2004, 2007; Rightmire et al., 2006) and paleoenvironmental change (Klein, 1972, 1976; Klein et al., 1983; Deacon and Lancaster, 1988).

Central to paleoanthropological research is an understanding of human land use and foraging behavior in the past. However, throughout the Middle and Late Pleistocene sea levels fluctuated dramatically making the modern coastal setting of these caves a poor analog for their time of Stone Age occupation. This is particularly true along the south coast of South Africa where the gradual slope of the Agulhas Bank means that when seas receded new land was exposed seaward of the caves (Van Andel, 1989) and ocean was replaced by landscapes of unknown floral and faunal character (Fig. 2).

The diverse array of environmental conditions likely experienced during the Middle and Late Pleistocene at these now-coastal caves provides compelling case studies to explore the relationship between human behavior and paleoenvironmental change across the South African landscape. But, terms like 'landscape' or 'seascape' impose epistemological limitations both thematically (i.e. land and sea) and also chronologically because without clarification these terms are often either derived from, or describe directly, the current environmental conditions. In places such as the southern coast of South Africa it is difficult to conceptualize the 'landscape' other than the now-coastal setting. Whether intentional or not, we believe that these terms (e.g. landscape and seascape) do introduce some bias into the perception of the area in the past, especially when the research focuses on times when the coastline differed from present conditions. Therefore, in this paper we rely on the 'paleoscape' as a heuristic research concept to situate the records for human evolution within a dynamic model of

* Corresponding author. Tel.: +1 480 965 1077.
E-mail address: erich.fisher@asu.edu (E.C. Fisher).

0277-3791/$ – see front matter © 2010 Elsevier Ltd. All rights reserved.
doi:10.1016/j.quascirev.2010.01.015

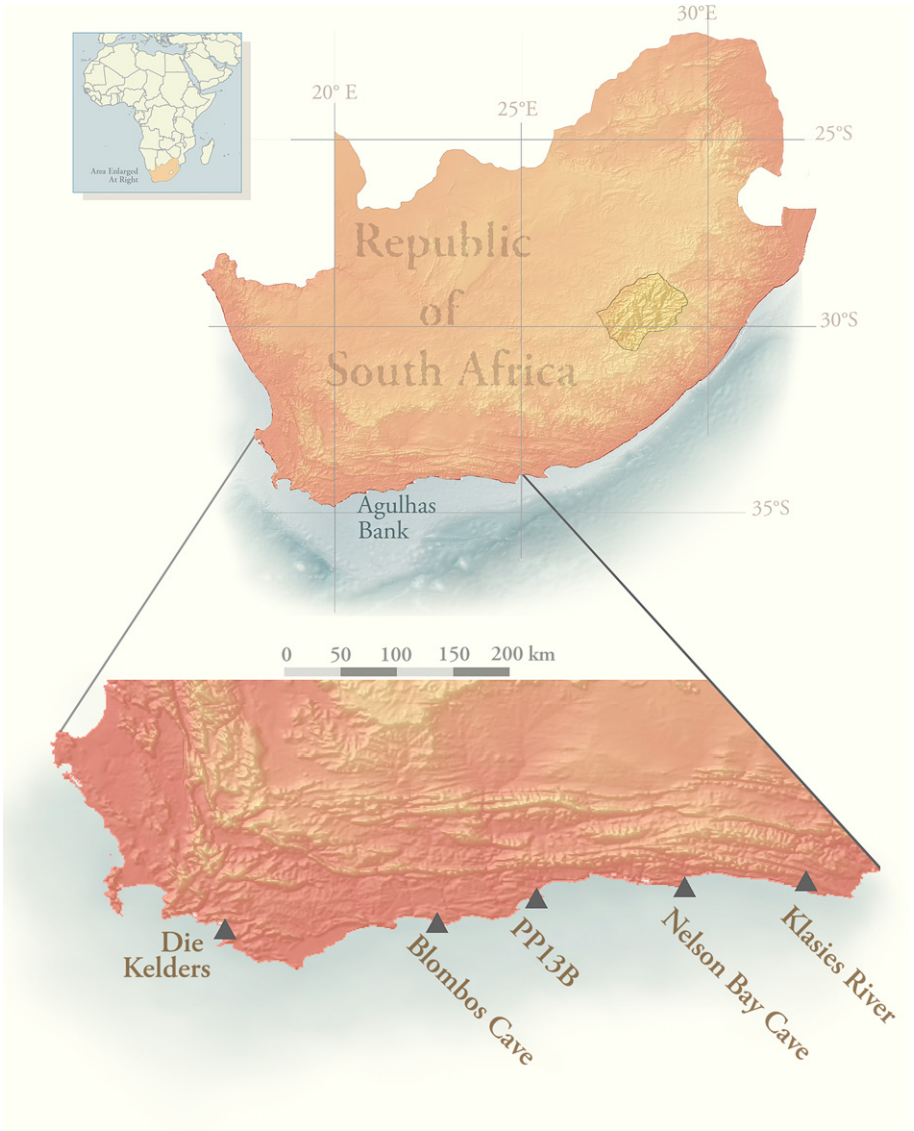

Fig. 1. Selected coastal MSA sites in South Africa that contain sedimentary and archaeological sequences that span the late Middle Pleistocene to the Holocene.

paleoenvironmental changes. This concept is especially useful within our research area because it helps researchers to associate the existing terrestrial and submerged environments into a single entity, independent of the current coastline configuration, upon which numerous elements, including sea level fluctuations, can be rendered dynamically to model past environments and to test hypotheses of environment – human behavioral interactions.

Here, we present a beginning paleoscape model at Pinnacle Point, South Africa (Western Cape Province) where a large number of caves and rockshelters contain a rich record of human occupation currently dated back to 174 ka and a sedimentary record that contains important geological evidence for paleoclimatic and paleoenvironmental change exceeding 800 ka. Pinnacle Point is currently a focus of the South African Coast Paleoclimate, Paleoenvironment, Paleocology, and Paleoanthropology Project (SACP4). SACP4 seeks to develop a high-resolution and continuous paleoclimatic and paleoenvironmental reconstruction of the south coast of South Africa from marine isotope stage (MIS) 11 through MIS 3 and contextualize within that reconstruction a detailed record of human adaptive change across the origins of modern humans. Developing a paleoscape model is a key component of that effort.

We are in the formative phase of developing the paleoscape model and one of our first goals is to accurately model how far the coastline is from our archaeological sites at relatively small temporal increments. This is because the coastline, and the Cape Floral Region (Goldblatt, 1997; Goldblatt and Manning, 2002; Cowling and Proches, 2005) that hugs that coastline, afforded a wide set of highly favorable food resources for ancient people. To understand the contribution of these resources to the human adaptive system during the crucial period of the origins of modern humans we need to understand the advance and retreat of the coast relative to the human foraging radius from the archaeological sites under investigation. We begin our focus at Pinnacle Point where we are concentrating our research, and compare the coastline predictions of the paleoscape coastline-distance model against an independent indicator of distance to the sea arguing that the changes in $^{87}Sr/^{86}Sr$ of speleothems and tufa depend on the distance of the caves from the shoreline. We then compare the model predictions against evidence for human coastal resource exploitation from MIS 6 through 5 at Pinnacle Point. Finally, we present an expanded, but lower resolution, paleoscape model and compare its predictions against the record for human occupation

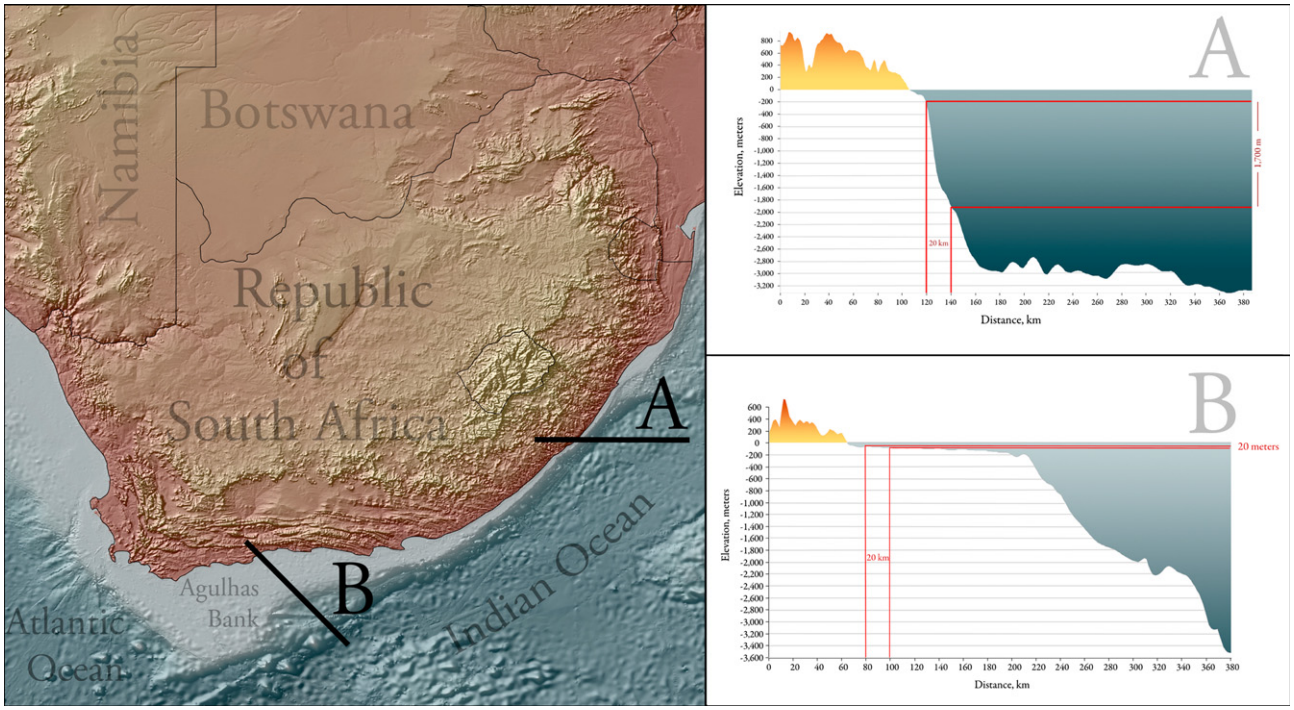

Fig. 2. The relationship between seafloor topography and changes in relative sea level height. The gradual sloping Agulhas Bank, off the coast of South Africa, means that large tracts of submerged land along the southern and western coastlines were exposed during sea level regressions.

at Blombos cave (Western Cape Province). Our work builds on prior seminal studies in South Africa on the relation between sea level, topography and human occupation by Hendey and Volman (1986) and Van Andel (1989).

2. The climatic and environmental context for the African origins of modern humans

The genetic and anatomical evidence suggests that *Homo sapiens* and the modern human genetic lineage arose sometime between 200 and 150 ka in Africa (Ingman et al., 2000; White et al., 2003; McDougall et al., 2005; Fagundes et al., 2007; Gonder et al., 2007). The technological phase during this event is known as the Middle Stone Age (MSA) in Africa and occurs between 300 and ~30 ka (McBrearty and Brooks, 2000; Marean and Assefa, 2005). Current archaeological evidence supports the hypothesis that a modern behavioral adaptation arose well prior to 40 ka in Africa and not as part of a late punctuated "Human Revolution" (McBrearty and Brooks, 2000; Marean and Assefa, 2005). At about 70 ka in South Africa several precocious forms of material culture appear including bone tools such as points (Henshilwood et al., 2001a; d'Errico and Henshilwood, 2007; Backwell and d'Errico, 2008), beads (Henshilwood et al., 2004; d'Errico et al., 2005), large quantities of worked and unworked pigments (Watts et al., 1999; Watts, 2002), decorated ochre (Henshilwood et al., 2002; Mackay and Welz, 2008), and heat treatment of lithics (Brown et al., 2009). There is now a resetting of the research focus to determine where, when, and why modern humans evolved, and much of that effort targets the interval between 200 and 50 ka, and coastal South Africa plays a prominent role in that endeavor.

In coastal areas, such as in South Africa, sea level changes during the Pleistocene not only affected the local environments and their human inhabitants (Van Andel, 1989), but it also served to alter the archaeological record (Hendey and Volman, 1986; Bailey and Flemming, 2008). Along the south coast of South Africa, a gently sloping and broad continental shelf (the Agulhas Bank) causes rapid coastline changes with even small vertical shifts in sea level height (Fig. 2b). Low sea stands during cold periods, therefore, would have produced substantial amounts of new land for habitation and potentially altered the flora and faunal resources of now-coastal areas. For much of the period from the origin point of the modern human lineage to the end of the MSA sea levels were lower (Jouzel et al., 2002; Waelbroeck et al., 2002), and thus the coastline was further from now-coastal sites than it is today. Populations were, undoubtedly, present out on exposed areas, likely drawn by the rich shellfish beds at the coast and the terrestrial faunal and floral communities on the exposed shelf. In other areas along the eastern and western South African coastlines a narrower continental shelf meant that less area was revealed during regressions and the amplitude of shifts on coastline change was reduced (Fig. 2a).

Conversely, high sea stands during warmer periods would have pushed sea levels higher up the current cliffs that abut the Holocene coastline, washing out the sedimentary records in caves situated below the mean sea level, inundating low-lying coastal plains, and relocating estuaries (Haas and Harrison, 1977; Hendey and Volman, 1986). The erosion of the sedimentary and archaeological records would have been enhanced further by high spring tides and storm surges during these times adding at least 2 m to the erosion zone. The MIS 5e (~128–110 ka) sea level was a likely candidate for intense erosion of sediments in low-lying caves and rockshelters (Hendey and Volman, 1986), as was the MIS 11 (~400 ka) high sea level (Olson and Hearty, 2009). Many deposits pre-dating these periods were likely substantial and some caves, such as Die Kelders Cave 1 (Marean, 2000) and the PP13 Site Complex (Marean et al., 2004, 2007), preserve remnants of these deposits cemented to their walls, cliff faces, and ceilings. The effect is that the sedimentary sequence can be, for the most part, reset to zero. The dual resetting by MIS 5e and MIS 11 partially explains the relative rarity of pre-120 ka and Acheulean cave and rockshelter occupations in coastal South Africa.

2.1. Pinnacle point

Pinnacle Point is a small promontory on a southward facing cliffed coast on the Indian Ocean, approximately 6 km west of the Mossel Bay point (Fig. 3). From Pinnacle Point to the Mossel Bay point, the heavily dissected coastal cliff displays caves, gorges, arches, and stacks that signal cliff dissection and retreat, a process enhanced by repeated high sea levels (Bird, 2000; Woodroffe, 2003). There are some small embayments along the rocky stretch, but nothing larger than a few hundred meters across. On the easternmost point of the cliffed coast is the point of Mossel Bay, a half-moon bay well protected from the prevailing southwesterly winds. Pinnacle Point is directly exposed to the sea.

The coastal cliffs are highly folded and faulted exposures of the Skurweberg Formation of the Paleozoic Table Mountain Sandstone Group. This formation comprises coarse-grained, light-gray quartzitic sandstone, with beds of varying thickness and consolidation, often covered with lichens. The dip varies strongly along the coast, ranging from 10 to 75° (South African Geological Series 3422AA 1993). Shear zones with *boudinage* features cut through the Table Mountain Sandstone (TMS), fault breccias of varying thickness fill these zones, and the caves and rockshelters are found in these eroded fault breccias. Unlithified dunes, aeolianites, calcarenites, and calcretes of the Bredasdorp Group cap the TMS throughout the area, and are mostly referable to the shallow marine Middle and Late Quaternary Klein Brak, and aeolian deposits of the Waenhuiskrans and Strandveld Formations (Malan, 1987, 1991). These are found in extant caves, in the remnants of collapsed caves, cemented to the cliff walls, and on the landscape. Sonar studies have shown that these dune systems are partially preserved on the submerged continental shelf and likely connected to the better preserved terrestrial systems at Sedgefield and Wilderness (Birch et al., 1978; Flemming, 1983; Flemming et al., 1983).

At Pinnacle Point, a large number of coastal caves (>20) occur in the nearly vertical cliffs in the thicker shear zones where substantial fault breccias have formed, and the caves typically coincide with less steeply dipping beds (10–40°). The primary mechanisms for cave development include the formation of the shear zones, followed by movement along these shear zones and erosion at the contact, cementation of the breccia, mechanical erosion by high sea levels, and in some cases collapse. The cave floors cluster at two heights; +3–7 m above mean sea level (amsl) and +12–15 m amsl. SACP4 has focused on the Pleistocene human occupation of several of these caves and rockshelters at Pinnacle Point (Marean et al., 2004, 2007).

3. Sea level modeling

During the Quaternary, cyclical variations of the orbit and rotation of the Earth created large-scale shifts in temperature that resulted in advances and retreats of polar ice (Bradley, 1999). When the climates are cooler more of the hydrosphere is trapped in the polar ice caps and sea levels drop (Shackleton and Opdyke, 1973). The opposite occurs during warmer periods. Eustatic changes in relative sea level (RSL) can be inferred from isotopic records from deep sea cores and ice cores (Chappell and Shackleton, 1986; Chappell et al., 1996). Continuous RSL curves developed for long time spans are most commonly built from isotopic methods, while onshore geological features provide more discrete snap-shots of ancient sea levels. All of these methods have their limitations and potential error (Caputo, 2007). The greatest weakness of the use of onshore geological features is the common inability of sea level modeling to accurately

Fig. 3. Location of caves at Pinnacle Point where speleothem samples were taken for this study. The cliffs at Pinnacle Point are approximately 50 m high. Areas at the base of the cliffs can be inundated by sea water during high tide but none of the caves are ever beyond ~10 m from the water line.

measure past uplift, or even the constancy of the uplift rates requiring assumptions to be made of the data (Caputo, 2007).

3.1. Glacio-isostatic influences

Given its latitudinal position, glacio-isostatic influence is highly unlikely for the south coast of South Africa. There is no evidence for Cenozoic volcanic activity and no deep seated heat source (de Wit, 2007) that would cause uplift. As Van Andel (1989) notes, the MIS 5e beach has been measured at approximately +4–6 m amsl throughout the South African coast (see also, Marker, 1984, 1987) which is in accord with more recent estimates of the MIS 5e high sea stand (Lambeck et al., 2002; Ramsay and Cooper, 2002; Hearty et al., 2007). This would suggest that along the coast of South Africa there appears to have been relatively little vertical crustal motion in at least the last several hundred thousand years.

3.2. Oxygen isotope RSL curves

Oxygen isotope ratios provide the most common source of RSL curves. Oceanic water is composed primarily of two of three stable oxygen isotopes, ^{16}O and ^{18}O. ^{16}O is lighter atomically than ^{18}O and is preferentially evaporated. Likewise, as oceanic water is consolidated into ice sheets during cooler periods the ice is primarily composed of lighter ^{16}O. The remaining sea water is more saline and enriched with the ^{18}O. The sea levels are also effectively lower thereby providing the link between the isotopes and sea level changes.

Once a relationship can be made between isotopic change and sea levels then the oxygen isotope data can be translated into relative sea level height. A common relationship is 0.1‰ $\delta^{18}O$ per 10 m sea level (Shackleton and Opdyke, 1973; Chappell and Shackleton, 1986; Shackleton, 1987; Jouzel et al., 2002). However, variability in the source data is a limitation in the use of oxygen isotope ratios and the localized nature of these data means that similarly timed oxygen isotope ratio data can produce different RSL curves, which may potentially alter interpretations made from those data (Caputo, 2007). Deep sea and ice core data are also orbitally tuned and this adds another substantial potential error between the age model of the RSL curve relative to observations in archeology and geology that are dated with techniques such as uranium–thorium (U–Th) and optically stimulated luminescence (OSL).

4. GIS modeling of RSL height and coastline morphology

It is important to first draw a distinction between modeling sea level heights, such as in RSL curves, and modeling coastline distance and morphology. The former is only a modeled measure of the vertical position of a mean sea level at a particular time. The latter is extrapolated from the vertical interlocation of RSL heights against bathymetry and terrestrial topography. In the past, many researchers relied on modeled RSL heights of low sea levels, which were plotted onto offshore topography, to estimate ancient shoreline positions and configurations. Van Andel (1989), for instance, focused on the −40 m, −75 m, and −120 m sea level heights as illustrative of major sea level regressions in the late Quaternary.

However, others have referred to RSL heights independently as a gauge for inferring coastline location without due consideration for the local offshore topography. Bailey (2007), for example, refers to a sea level curve spanning the last 140,000 years to denote the likely visibility of marine resources during the +5 m MIS 5e high sea stand (~120 ka) and −20 m low sea stand (~80 ka) at the now-coastal South African MSA sites of Blombos and Klasies River, among others. But, by disregarding the local terrestrial and bathymetric topography adjacent to those sites their approach must assume the topology between the site as a fixed point on land, the coastline, and the seafloor. The danger in this approach is as noted prior: as RSL height changes the slope of the offshore topography can profoundly affect coastline movements or hardly affect the coastline location at all (Fig. 2).

We build on prior approaches to coastline modeling in several ways. First, our goal is to create a dynamic computer model based within a GIS framework that allows us to model coastline distance and configuration at user-defined increments and free us from being tied to more static estimates. For example, if our archaeological ages reveal site occupation at about 110 ka, we want to input 110 ka and get an immediate result.

Second, we want a model that is organic in that as the input data improves (bathymetry, the sea level curve, regional sea level estimates from geological features, etc.) those improvements can be rapidly added to the model. Used in tandem, these features provide the framework for our model and they can be experienced more fully in the accompanying Supplementary Video. Production information for the Supplementary Video can be found in the Supplementary Materials, section 5.

Our current paleoscape model is founded on a dynamic model of the coastline relative to the current local bathymetry over the length of our problem orientation (~430–30 ka). We have used this model to interpolate an array of distances to the coastline from site PP13B. To accomplish this, we started with a reconstructed RSL curve developed by Waelbroeck et al. (2002) to model sea levels at Pinnacle Point during the Pleistocene. We chose this curve because it is the most recent, complete, and lengthy of the published RSL curves, though our model could be constructed with any curve available.

4.1. The RSL curve

The reconstructed RSL curve developed by Waelbroeck et al. (2002) was extrapolated from oxygen isotope ratios from benthic foraminifera in the north Atlantic, south Indian, and equatorial Pacific oceans and spans the last 430,000 years in 1500-year increments. Core samples <40 ka were dated by ^{14}C while samples >40 ka were correlated to the Imbrie et al. (1984) and Martinson et al. (1987) SPECMAP reference stacks (Waelbroeck et al., 2002). At the MIS 5–6 transition, the SPECMAP ages were adjusted to conform to U–Th aged RSL data. Dating errors range between 1 and 4 ka prior to 40 ka and decrease to 500–800 years during the last deglaciation. RSL error is <±13 m, but within the last 200 ka it is likely to be much less. We have begun to correlate this composite sea level curve to our field measurements of local geological indicators of prior high sea stands (MIS 5e and 11) to fine tune the globally-designed model of Waelbroeck et al. (2002) to our locality. While we have noted some minor vertical disagreement, in general, Waelbroeck et al. (2002) reconstructed RSL curve accords well with our local geological data.

4.2. Elevation models

All elevation data were transformed into the South African National Grid system (Lo.23) to accommodate the geodetic format of most locally available mapping data in South Africa. Projection and geographic coordinate system parameters for the South Africa National Grid are provided in the Supplementary Materials, section 1.1. Base terrestrial elevations are a combination of mosaicked regional WRS-2 C-band unfilled and unfinished SRTM 90 m digital elevation data[1] (USGS, 2004) and local discrete point data which

[1] Data was acquired from the Global Land cover change Facility (GLCF), www.landcover.org.

were derived from 1:5000 scale aerial photographs of the Pinnacle Point area[2] taken during a planning phase for a local development. These data are further supplemented by nearly 100,000 total station shots taken by SACP4 personnel with centimetric accuracy of the cliff faces around Pinnacle Point.

Bathymetry elevations are a compilation of digitized 5 m vertical-interval contour maps up to 100 km from Pinnacle Point[3] supplemented with a systematic grid of 340 m horizontally spaced side-scanning SONAR data points within 20 km of the Pinnacle Point shoreline.[4] The lowest resolution bathymetry data (340 m) is considered here to be the minimum expected error within the coastline model predictions. But, when we compare the actual current mean sea level coastline against our modeled current mean sea level coastline we find there is ~85 m horizontal difference between the two. We therefore consider 85 m to be our working horizontal positional error within our coastline models. Since these estimates are each less than 0.5 km, the influence of these errors upon our coastlines predictions is considered negligible to any conclusions derived there from and is thus not included in the distances described below.

We used the ESRI ArcGIS 9.3 Geostatistical Analyst to generate the bathymetric elevation model and cross-validation statistics. The elevation model is based on the ordinary kriging method, which was employed because it offers robust statistics to explore the fit of the model against the input data point set. The multiple data sources, their various collections methods, inherent errors, and resolutions, however, meant that a perfect fit of our model to the input points was highly unlikely. We estimated that a maximum mean error of 5 m between the original and derived bathymetric point locations was within the tolerance limits of the data and offered sufficient minimum resolution for our purposes.

The bathymetric point set was best fit using an exponential semivariogram. Adjustments to the lag size, anistrophy, and number of neighbors were able to resolve a model with a mean prediction error of −0.035 m between the original and derived model elevation values. The standard deviation (i.e. RMS) of the mean prediction error was 2.56 m. The full array of the model validation results are provided in the Supplementary Materials, section 2.1. The bathymetric and terrestrial elevations models were subsequently mosaicked into a single, continuous comprehensive elevation model.

4.3. GIS processing the paleoscape model

By correlating each vertical sea level value from Waelbroeck et al. (2002) reconstructed RSL curve to our comprehensive elevation model around Pinnacle Point, we were able to model sea levels and their shorelines in the past. Thus if each vertical sea level height within the RSL curve represents a level plane then the intersection of this plane against local bathymetric and terrestrial elevation data provides a generalized location of the coastline at that period in the past.

We used a custom Python 2.5 script to batch geo-process each of the 288 1500-year increment vertical sea level values provided by Waelbroeck et al. (2002). The script iterates by line within a predefined list of sea levels and corresponding ages and performs the following processes in order:

1. Extracts raster values less than the predefined sea level value.
2. Reclassifies each of the extracted raster values to the original sea level value.
3. Converts the raster data into a new Z-aware (3D) polygon where the polygon Z-value is set to the sea level height.
4. Names each new Z-aware polygon file based on the sea level height and age (e.g. file s167k-49_53.shp represents the −49.53 m asl sea level at 167.0 ka).

In this manner each final Z-aware polygon is pre-calibrated to the exact sea level height, clipped precisely against the original elevation data, and shows where the coastlines likely were located in the past. All derived data within the GIS conform to the South African National Grid system (Lo.23).

We then used a calibrated route (a linear feature with a predefined measurement system) to calculate Euclidian distances between cave PP13B at Pinnacle Point (cf Marean et al., 2004, 2007) and each modeled coastline within the GIS. The route was oriented 150°, which is approximately perpendicular to the cliff aspect around Pinnacle Point, and it stretched from PP13B to slightly beyond the farthest modeled coastline, 124 km distant. Distance data reported upon here is provided in tables described below based on the 150° bearing; the full array of mean, maximum, and minimum coastline distances is provided in the Supplementary Materials, section 3.1.

It should be noted, however, that 150° is really only an arbitrary bearing, and because of surface variations across the Agulhas Bank, it may not reflect the actual nearest or farthest extent of each coastline from PP13B. To determine the amount of potential variation in our model we also mapped coastline distances along a profile route extending due south (180°) from PP13B. The paired array of data values (150° and 180°, respectively) was compared using a one-tailed Spearman's rho correlation. The results of this test show that the two models share 99.2% of their ranked variation ($p < .01$). This is due to the similar near-shore topography of the Agulhas Bank. It is only beyond 30–50 km from PP13B when topographical differences appear to effect ±10 km differences in coastline predictions.

5. $^{87}SR/^{86}SR$ isotope ratio data

The use of $^{87}Sr/^{86}Sr$ isotope ratios in speleothems has been shown to provide important information about atmospheric circulation, the origin of dust, and weathering processes (Banner et al., 1996; Goede et al., 1998; Ayalon et al., 1999; Bar-Matthews et al., 1999; Verhyden et al., 2000; Frumkin and Stein, 2004; Musgrove and Banner, 2004). In this study we explore the use of $^{87}Sr/^{86}Sr$ isotope ratio data as a potentially effective proxy for coastline distance over time. We test the hypothesis that $^{87}Sr/^{86}Sr$ ratio values closer to that of sea water characterize speleothems that were deposited when sea levels were higher and thus located closer to the sample location of the cave. This relationship is founded in the contribution of sea-derived spray, mist, and fog to the seepage water from which the speleothems are formed. Modern sea water has a $^{87}Sr/^{86}Sr$ ratio value of 0.7092 and deviation from this value in the speleothem indicates a less dominant contribution of sea-derived spray to the seepage waters, likely because of increased distance between the speleothem and the coastline. At Pinnacle Point, for example, the $^{87}Sr/^{86}Sr$ isotope ratios of speleothems deposited during the last 300 ka have values ranging between 0.7092 (modern sea water value) and 0.7095. Since the speleothem samples are also precisely dated we are able

[2] The aerial survey was conducted in 2002 by Photosurveys (Cape) Pty Ltd. The photography was collected at an elevation of 2,500 feet using a Zeiss RMK Top camera (focal length 152.346 mm), digitized with a Vexel photogrammetric scanner (25 μ), and adjusted using "PAT B" aerial triangulation software. Points were derived from these images using a manually operated Soft Copy Photogrammetry work station with field-checked accuracy of the points being within 0.10 m.

[3] Data provided by T. van Andel

[4] Data provided by C. Bosman, Council for Geoscience, South Africa: Marine Geoscience Unit

to further statistically compare the modeled coastline output generated from our paleoscape model to the measured and dated $^{87}Sr/^{86}Sr$ ratios from 320 ka to the present.

5.1. Speleothem sample locations

All speleothem samples described here are from well studied caves around Pinnacle Point (Fig. 3). The timing of speleothem deposition at these sites is well constrained by U–Th dating and $\delta^{18}O$ and $\delta^{13}C$ isotope compositions of each sample were further analyzed for additional paleoclimatic research (Bar-Matthews et al., 2008). All of the caves are within 1 km of one another, within 50 m of the current high tide mark, and their mouths face the sea. Descriptions of the caves are provided below.

At various times the caves were closed or partially closed by dunes that formed against the cliff face and in some cases these lithified into aeolianites cemented against the cliffs. Our definition of "closed" thus includes situations when the opening was completely or nearly completely blocked by sand or cemented sand. These conditions are diagnosed when the speleothem that is formed is clean and detritus-free. During times when the caves are open, tufa is formed. The tufa and clean speleothem diagnoses were done from the chemistry and optical microscope analyses at the Geological Survey of Israel. Remnants of these aeolianites and their surfaces are preserved at many locations. At other times the caves were open or partially open, at which time some were inhabited by people and others by animals (Marean et al., 2004, 2007). We note below when we estimate that caves were open and closed, and this is based on geological reconstructions derived from field studies, petrography, 3D modeling of studied and dated features (speleothems and sediments), optically stimulated luminescence dating, and U–Th dating of clean speleothems and tufas.

5.1.1. Crevice cave

This cave, currently open, has no archaeological remains, but has remnant aeolianite as well as thick flowstones, stalagmites, and stalactites. The Lower cave has been the focus of an intensive $\delta^{18}O$ and $\delta^{13}C$ study, and was closed between ~90 ka and 53 ka (Bar-Matthews et al., 2008). There are deposits on the cliff face above that we call Crevice Cave Upper because the formation of speleothem clearly shows the ancient presence of caves, now eroded to small pockets and fissures.

5.1.2. PP9

This large cave, currently open, includes archaeological deposits, extensive dunes, as well as speleothem.

5.1.3. PP13B

This cave, currently open, has a rich archaeological record of human habitation, but also several phases of closure and near closure when speleothem grew. It was closed between ~90 and ~40 ka and there appears to have been an earlier phase of closure or partial closure ~220 ka, but of uncertain duration.

5.1.4. PP13F

This cave, currently open, has no clear archaeological remains, but remnant features of speleothem and aeolianite show clearly that this cave also had periods of closure and near closure. It was closed between ~90 ka and ~28 ka.

5.1.5. Staircase cave

This now-collapsed cave is visible only by small remnant deposits of cave sediments, aeolianite, and speleothem adhering to the cliff face. This is one of the oldest caves at Pinnacle Point and it had phases of closure and speleothem formation from before the limit of U–Th dating (~500 ka) to ~155 ka, sometime after which it collapsed.

5.2. Methods

The speleothem samples were taken by various methods (core, rock hammer, diamond chain saw, and angle grinder) between 2000 and 2008. All U–Th and strontium analyses were conducted at the Geological Survey of Israel. ^{230}Th–U dating was performed on all speleothem samples using multicollector inductively coupled plasma mass spectrometer (MC-ICP-MS) Nu Instruments Ltd (UK) equipped with 12 Faraday cups and 3 ion-counters. The sample was introduced to the MC-ICP-MS through an Aridus® micro-concentric desolvating nebulizer sample introducing system. The instrumental mass bias was corrected (using exponential equation) by measuring the $^{235}U/^{238}U$ ratio and correcting with the natural $^{235}U/^{238}U$ ratio. The calibration of ion-counters relative to Faraday cups was performed using several cycles of measurement with different collector configurations in each particular analysis. The age determination was possible due to the accurate determination of ^{234}U and ^{230}Th concentrations by isotope dilution analysis using the ^{236}U–^{229}Th spike.

For strontium analyses ~50–100 mg of each Sr isotope sample was dissolved in HNO_3 with the strength of the nitric acid dependent upon the Sr concentration. The final concentration was 3.5 N HNO_3. This was loaded onto a 0.5 cc resin column containing Eichrom-Sr-spec Resin (50–100 mesh). The matrix was rinsed with 3 portions of 1 ml 3.5 M HNO_3 and one portion of 0.5 ml 3.5 M HNO_3. Sr was eluted by 3 × 1 ml 0.05 M HNO_3. The $^{87}Sr/^{86}Sr$ isotopic composition was measured following published protocols (Ehrlich et al., 2001; Halicz et al., 2008). 5 Faraday collectors were used for measurements of masses: 83 (Kr), 85 (Rb) and 86, 87, 88 (Sr). ^{83}Kr was measured in order to correct for ^{86}Kr interference due to Kr contamination in the Ar gas. ^{85}Rb was measured in order to correct for ^{87}Rb interference. ^{87}Rb was calculated from the ratio of $^{87}Rb = 0.3860 \times {}^{85}Rb$, after mass bias discrimination correction with the exponential law. The correction factor is calculated from the measured $^{87}Sr/^{86}Sr$ ratio, employing the exponential law mass bias correction using the $^{87}Sr/^{86}Sr$ natural ratio of 0.1194. Error on Sr isotopic ratios is 0.00001–0.00002 at 2-sigma. All separation procedures were performed in an ultra clean lab, using standards and blanks to verify that there is no contamination. The complete data set of U–Th and strontium data are provided in the Supplementary Materials, section 4.1.

5.3. Analysis of $^{87}Sr/^{86}Sr$ isotope ratio data

Our composite sequence is derived from 132 coeval $^{87}Sr/^{86}Sr$ measurements and U–Th ages spread between 1.5 ka and 325 ka. The $^{87}Sr/^{86}Sr$ ratios vary between 0.70921 and 0.70965. Descriptive statistics of the $^{87}Sr/^{86}Sr$ ratio data as well as summaries of the $^{87}Sr/^{86}Sr$ measurements from each study site, and also grouped by 10 ka classes, can be found in the Supplementary Materials, section 4.2. Our record has its densest set of measurements between 140 and 40 ka when conditions were optimal for clean speleothem growth in the various caves. Beyond this range the analyses are spread much thinner due to the absence of available speleothem.

The uneven spread of the Sr data required that we smooth (loess technique, sampling proportion = 0.1) to scale the Sr data similarly to the coastline distance output of the paleoscape model. We employed the loess method as it performs well with unevenly spaced data. Fig. 4 shows our modeled coastline distances from PP13B compared to the loess smoothed $^{87}Sr/^{86}Sr$ ratio. Overall, the pattern of $^{87}Sr/^{86}Sr$ ratios tracks closely to the pattern in the distance to the coastline. There are clear offsets between the peaks

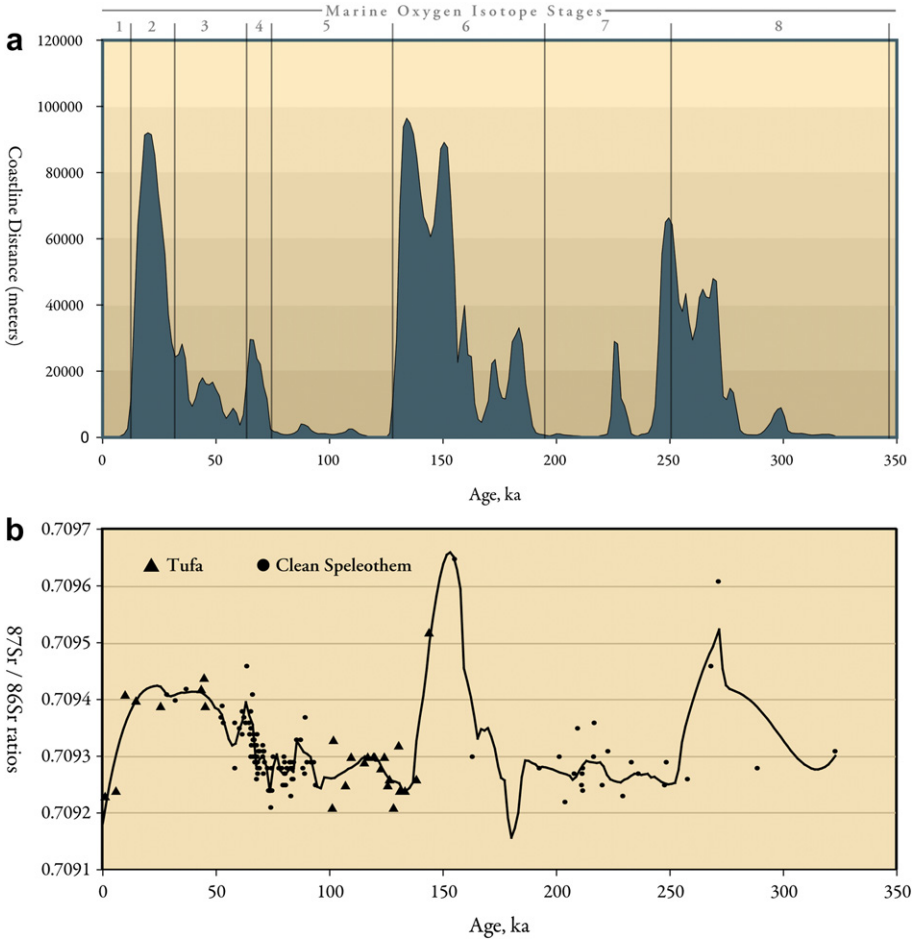

Fig. 4. a and b. The smoothed $^{87}Sr/^{86}Sr$ ratios compared to the coastline distance. The upper graph (4a) shows the fluctuation of coastline distance at Pinnacle Point within the last 323 ka, which is the lower limit of the $^{87}Sr/^{86}Sr$ data. MIS Stages (Bradley, 1999:212, following Shackleton and Opdyke, 1973) are superposed for reference. The lower graph (4b) shows the Crevice Cave $^{87}Sr/^{86}Sr$ loess curve with the original $^{87}Sr/^{86}Sr$ points. Tufa speleothem samples are identified as triangles and clean speleothem as circles.

and troughs, but it is important to note that the majority of the coastline distance curve is globally tuned while our $^{87}Sr/^{86}Sr$ ratios curve is directly dated and there could be substantial dating offsets by that fact alone. We are not yet at the stage where we can correct the ages of the paleoscape model based on the terrestrial data, but we hope to do that in the future.

Using the output of the loess smoothed $^{87}Sr/^{86}Sr$ ratios, we investigated the correlation between the coastline distance and the Sr data. While there is clearly a tendency for the $^{87}Sr/^{86}Sr$ ratios to increase with distance from the coast (Fig. 4), a visual inspection of the scatter (Fig. 5a) shows that a linear regression model is probably inappropriate. Furthermore, while the relationship is significant, the r^2 is also rather low ($r^2 = 0.1986$, $p < .0001$). To explore this result, we conducted the regression analysis on the clean speleothem only. Our reason for doing so was to explore the potential that the Sr of clean speleothem and tufa may be responding differently because tufa is forming when the caves are at least partially open, and thus subject to direct sea spray input. Eliminating tufa from clean speleothem results in a better fit to the regression model (Fig. 5b) as the $^{87}Sr/^{86}Sr$ ratios of the clean speleothem shows a compelling tendency to increase with distance from coast ($r^2 = 0.3281$, $p < .0001$).

An analysis of residuals did not reveal any age-related pattern in predicted $^{87}Sr/^{86}Sr$ ratios relative to coast distance. However, an inspection of the standardized residuals (Fig. 6) does indicate that the highest deviations from predicted values (both negative and positive) occur during periods of rapid regression or transgression. This is what would be expected if the globally-tuned paleoscape model is offset from the U–Th based age model: large deviations would occur at periods of rapid change and then the relationship would fall into sync, and residuals drop, during periods of relative stasis. Overall, the $^{87}Sr/^{86}Sr$ ratios and distance to coastline for clean speleothem correlate well and will be eventually improved by refinement of the globally tuned age model used for the paleoscape model.

5.4. Summary of $^{87}Sr/^{86}Sr$ isotope ratio data and coastline distance

The patterns in $^{87}Sr/^{86}Sr$ ratios and coastline distance can be summarized as follows, starting at ~290 ka when the strontium record begins to increase in detail:

1. $^{87}Sr/^{86}Sr$ ratios increase from 0.70928 at ~288 ka to 0.70961 at ~271 ka. At approximately the same time the paleoscape model shows the coastline entering a regressive phase that shifts the coastline from nearer to the cliffs at 290 ka to 38–65 km distant by 272–245 ka.
2. From 258 ka to 200 ka $^{87}Sr/^{86}Sr$ ratios remain rather low and stable – varying between 0.70922 and 0.70936 – while the paleoscape model shows a broad transgressive phase at the same time. The synchrony of the records during this time is punctuated by a brief regressive spike centered at 225 ka which is visible in the paleoscape model but is not reflected in the

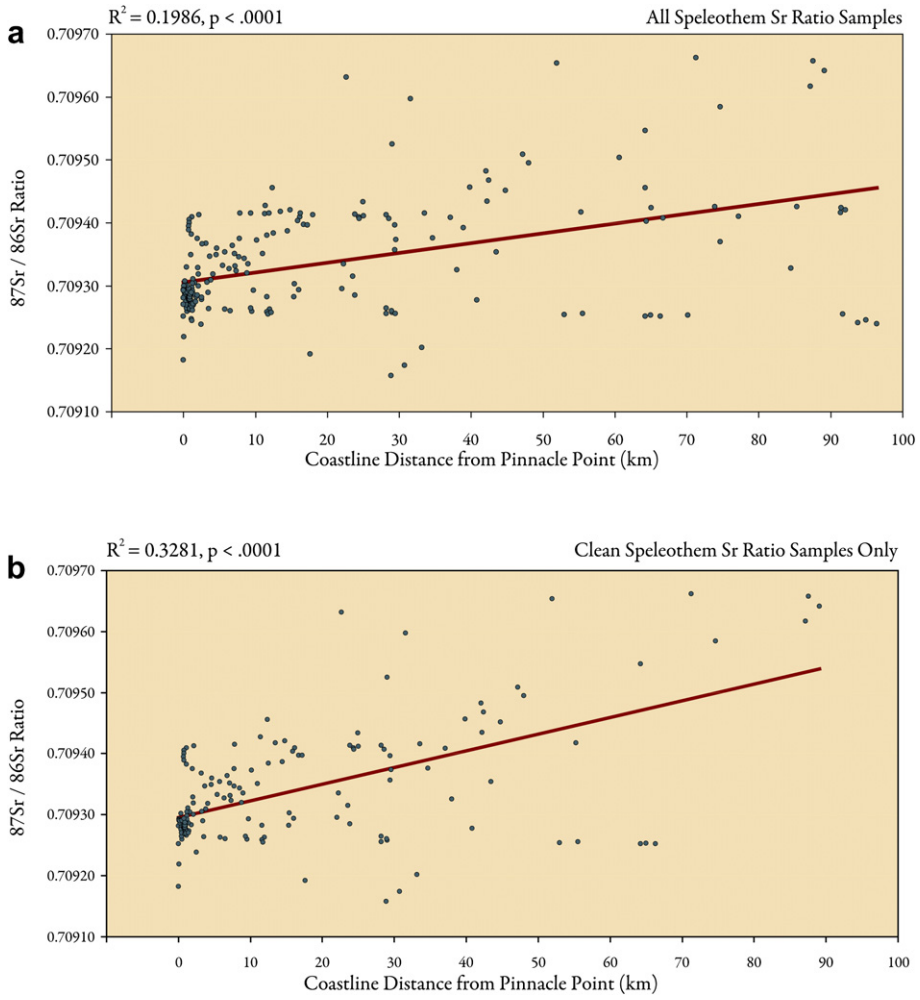

Fig. 5. a and b. Linear regression results of the smoothed Sr ratio samples and coastline distances. a. (upper) includes all Sr ratio samples. b. (lower) only includes Sr ratio data derived from clean speleothem samples when PP13B was closed.

$^{87}Sr/^{86}Sr$ ratios record. After 250 ka, changes in the $^{87}Sr/^{86}Sr$ ratio values typically lead the paleoscape model by ~6–12 ka.

3. Between 190 and 150 ka (MIS 6), the $^{87}Sr/^{86}Sr$ ratio record shows two minor regressive events, centered at 189.7 ka and 173 ka, but given the uncertainties in age and the low number of measurements in this time span, it is difficult to directly correlate the two events. These may be independent events considering that the paleoscape model also shows the coastline regressing twice beyond 20 km from Pinnacle Point during this time with maxima centered at 184.5 ka and 151 ka.
4. The coastline-distance model shows a brief transgressive event at ~167 ka that moves the coastline within 10 km of Pinnacle Point. The Sr data also shows a shift that indicates a short transgression at this same time. As note previously, the archaeological evidence shows that PP13B is reoccupied by people exploiting coastal resources at this time (cf Marean et al., 2007).
5. The $^{87}Sr/^{86}Sr$ ratio data and the paleoscape model each record a major regressive event associated with the end of MIS 6. The paleoscape model records two regressive peaks (maxima at 150.5 ka and 134 ka) with coastline distances nearly in excess of 100 km from Pinnacle Point. The $^{87}Sr/^{86}Sr$ ratio record shows only a single, broad maximum between 150.5 and 155 ka with the most radiogenic $^{87}Sr/^{86}Sr$ ratio values in the data set occurring at ~152 ka (0.70967). Despite the lack of correspondence in resolved peaks, the overall correspondence is outstanding.
6. By ~130 ka, the paleoscape model shows that the coast had moved within 1 km of Pinnacle Point, meaning that the average speed of this transgression was over 20 km per millennia. A maximum transgression velocity of 40 km per millennia was likely reached between 135 and 136 ka.
7. Both records display the rapid rise in sea levels associated with MIS 5 and the paleoscape model and $^{87}Sr/^{86}Sr$ ratios each show the coast at or near the cliffs. At ~72 ka, the paleoscape model and the $87Sr/^{86}Sr$ ratios each show a regression, followed by a short transgression at ~60 ka. The records are in sync until about 40 ka, after which the resolution of the $^{87}Sr/^{86}Sr$ declines and the massive LGM regression shown by the paleoscape model is not captured.

In summation, there are subtle differences in the timing and the character of the fluctuations within each data set. The $^{87}Sr/^{86}Sr$ records often lead the paleoscape model by 6–12 ka. Furthermore, the paleoscape model appears to be more sensitive to short-term sea level changes that appear as broader events within the $^{87}Sr/^{86}Sr$ record. Despite these differences, which we consider negligible and prone to refinement, the $^{87}Sr/^{86}Sr$ sequence does appear to correspond to changes in the distance of the coastline

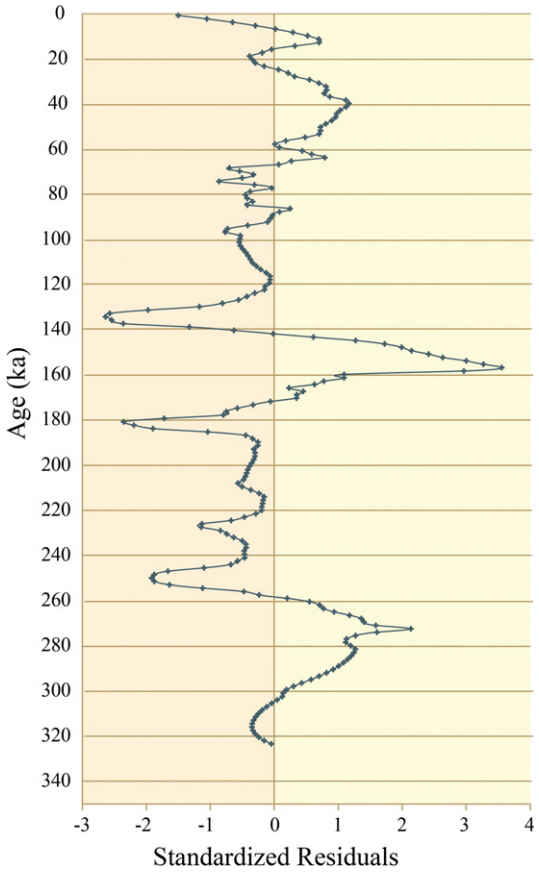

Fig. 6. Standardized residual values for the $^{87}Sr/^{86}Sr$ data by age derived from samples from Pinnacle Point caves, by age. The highest deviations in standardized residual values from predicted values (both negative and positive) occur during periods of rapid regression or transgression.

from the sample location. This would indicate a robust fit between the $^{87}Sr/^{86}Sr$ sequence and the paleoscape coastline model.

6. Shellfish exploitation and radiometric age estimates

Studies of hunter-gatherer mobility show that it is useful to distinguish between the annual home range (the area used by a group within a year), the daily foraging radius (the area surrounding a residential site that can be exploited in one daily trip), and a logistical foraging radius (that area exploited from a residential site with functionally specific sub-groups for trips longer than one night) (Binford, 1980, 1982; Kelly, 1983, 1995). Hunter-gatherers living in environments similar to the Cape region of South Africa (i.e. warm and dry) typically do not practice long distance logistical forays, so the use of space around a residential site is dominated by single-day foraging trips with a radius distance defined by what a person can walk out and back in one day, typically 8–10 km (Binford, 1980, 1982; Kelly, 1995). This is well illustrated in Khoi San ethnography (Lee et al., 1968; Lee, 1972; Tanaka, 1980; Silberbauer, 1981).

According to ethnographic observations (Meehan, 1982) and data gathered from Later Stone Age (LSA) sites along the West Coast of South Africa (Buchanan et al., 1984; Parkington et al., 1988; Jerardino, 2003) and other locations worldwide (Erlandson, 2001), shellfish collecting rounds tend to follow the daily foraging radius pattern. Thus, people travel to the coast to collect shellfish and then transport the catch back to the residential site when the distance is within 5 km, with a few rare cases exceeding 10 km (Bailey and Craighead, 2003; Jerardino, 2003). Furthermore, the longer the trip, the more likely that shellfish will be field processed (shucked) in close proximity to the beach. In this situation, the shellfish may be either eaten on location or the flesh could be possibly dried and transported to the residential site thereby leaving no physical remains at the residential location (Henshilwood et al., 1994; Bird and Bliege-Bird, 1997; Bird et al., 2002). It is likely that similar movement and transport distances characterized shellfish collectors during MSA times and here we assume that is the case given the consistency above between ethnography, LSA foraging strategy, and anthropological theory. The implication being that the presence of reasonably well-developed shellfish deposits in coastal MSA sites is an indication that the coastline was within sufficient distance (i.e. 5–10 km) that made shellfish collection and transport an activity worth pursuing from that location for MSA groups.

6.1. Radiometric age precision and accuracy

Current radiometric techniques that cover the MSA time span, and are regularly applied in South Africa, include thermoluminesence (TL) (Tribolo et al., 2006, 2009), optically stimulated luminescence (OSL) (Jacobs and Roberts, 2007; Jacobs et al., 2008), and electron spin resonance (ESR) (Grün et al., 2003). U–Th dating is not regularly applied in coastal South Africa, though some applications show its great potential when speleothem is intercalated with archaeological deposits (Vogel et al., 2001; Marean et al., 2007). With the exception of U–Th applied to clean calcite from a closed system (e.g. speleothem), the typical reported 1-sigma error on the former three techniques can be a significant time span, often on the order of 10% of the reported age. However, many of these techniques have still not been systematically applied to MSA sites so many of the coastal MSA South African sites remain essentially undated. Furthermore, many of these techniques continue to be subject to difficult modeling of past dose rates and moisture levels, and particularly TL and ESR continue to regularly provide age estimates that are often highly variable even within the same strata. Independent checks of these dates remain a high priority. We suggest that modeling sea level changes around specific locations of coastal MSA sites and the presence of well-developed shell lenses in their sequences can act as an independent check on chronometric determinations on shell-bearing MSA deposits. We provide an example below.

6.2. LC-MSA deposits at PP13B

The archaeological deposits at PP13B allow us to illustrate this approach. The cave is currently +13 m amsl at the mouth, and a rocky inter-tidal zone of the Indian Ocean is just below the mouth. Excavations and results are reported elsewhere (Marean et al., 2004, 2007). The entire set of deposits with anthropogenic material dates between ~174 and 91 ka, at which time the site was closed by a dune forming against the cliff face. Excavations were conducted in the north-eastern, eastern, and western areas of the cave. Shellfish are well represented in 4 major stratigraphic units, while many other stratigraphic units lack shellfish or have them in very low frequencies. The four units with significant amounts of shellfish include the LC-MSA Lower, LC-MSA Middle, LC-MSA Upper (reported on in Marean et al., 2007), and the Upper Roof Spall/Shelly Brown Sand unit (Jerardino and Marean, in press). The former 3 units are uniformly dominated by brown mussel (*Perna perna*), a rocky inter-tidal species common to the south coast. The Upper Roof Spall/Shelly Brown Sand is dominated by the sand mussel (*Donax serra*), a denizen of calm sandy beaches, but also

contains *P. perna* and small frequencies of limpets and *Turbo sarmaticus* (Jerardino and Marean, in press).

The chronology of the PP13B sediments is developed from OSL and U–Th dating. The OSL results are described in Jacobs (submitted for publication) and Marean et al. (2007, in press), while the U–Th results are described in Marean et al. (2007, in press), and the following summary is developed from those data. A conservative age spread is provided by taking the minimum and maximum OSL ages from each stratigraphic unit, and adding 1 sigma to each, and then adjusting these for U–Th ages that are intercalated. For example, the more precise U–Th ages on clean speleothems directly contacting the top of the archaeological sediments shows us that the cave closed no later than 91 ka, so that age is used to adjust the age span of underlying OSL-dated sediments to no younger than 91 ka. The LC-MSA Lower conservative age spread is 174–153 ka, the LC-MSA Middle is 130–120 ka, the LC-MSA Upper is 133–115 ka, and the Upper Roof Spall/Shelly Brown Sand is 98–91 ka.

6.3. Discussion

Of the four stratigraphic aggregates (LC-MSA Lower, Middle, Upper, and Upper Roof Spall/Shelly Brown Sand), it is the LC-MSA Lower that provides the greatest challenge to the paleoscape model. This is because the LC-MSA Lower falls within MIS 6 when published sea level curves predict very low sea levels. In fact, our paleoscape model suggests that the coastline would have been too far from PP13B for shellfish exploitation during nearly 98% of the approximately 67,000 year duration of MIS 6. This leaves 2% of the time period, approximately 1300 years, that the coastline was within 8 km of PP13B. Thus, to say that PP13B was consistently "many kilometers inland" during MIS 6, like Bailey and Flemming (2008:2156) have suggested,[5] is too generalized because it does not take into account sea level and coastline fluctuations that likely did occur during this time, which we can test through our model.

Table 1 provides the numerical distance from PP13B to the shoreline at each modeled 1.5 ka increment, including the modeled distances for the upper and lower sea level height errors given in the isotopes curve. In order to be concordant with the expected range of shellfish exploitation, the mean coastline distance, at least, must be within a maximum of 8 km from PP13B within the 2-sigma span of the age estimate as the dated deposits in question contain marine shell.

The results of our comparison show that sea levels regress at the end of MIS 7 (~195 ka) and continue to regress until 137 ka when average coastline distance to PP13B was nearly 100 km. However, the paleoscape model does record a brief transgression starting by 171.5 ka, and reaching a maximum 167 ka, which is concordant with the LC-MSA Lower. At this time (167 ka) the average distance to the coastline is 4.81 km, according to the 150° route calculations. The 180° route calculations suggest that the average coastline is only 1.38 km farther (6.19 km). Thus both routes model the average coastline distance within the 8 km daily foraging radius for shellfish exploitation at 167 ka and this likely lasted between168.5 ka and 165.5 ka. Coastline distances derived from the maximum isotopically-derived sea level heights[6] during this brief period, however, never fall below the 8 km limit,[7] but the maximum distance at 167 km (9.16 km) would only require a −2 m drop in sea levels to be within 8 km of PP13B. Coastline distances within the 8 km foraging radius that are derived from the minimum isotopically-derived sea level heights cover a much broader span of time between 177.5 and 164 ka.

As for the LC-MSA Upper in MIS 5e and the subsequent Upper Roof Spall/Shelly Brown Sand in MIS 5c-d, average distance from PP13B to the coastline never exceeded 4 km and likely ranged within 1 km most of the time. Sea levels were lower at the beginning of the LC-MSA Middle but the coastlines had transgressed to within 1 km average distance to PP13B by ~131 ka. Interestingly, the shellfish species composition and overall shellfish frequencies between the deposits can also be explained with our paleoscape model. Current observations on the PP13B marine shell assemblage show that the highest shell densities for the entire occupational sequence occur within MIS 5 when the coastline is predictably at its closest to the site as a result of highest sea levels (Jerardino and Marean, in press). Furthermore, sea levels were unstable during MIS 5c–d and there appears to be a brief, and rapid, regressive event starting ~99 ka and centered at 87.5 ka. Throughout this regressive event, the coastlines moved on average >0.5 km/1.5 ka and by 90.5 ka, these movements peak at nearly 1.2 km/1.5 ka. These predicted rapid regressive coastline movements are likely to have promoted the formation of dunes and exposed sandy beaches, the latter being the particular environment where *D. serra* populations thrive. The shellfish species composition of the Upper Roof Spall/Shelly Brown Sand is dominated by *D. serra*, an observation entirely congruent with our paleoscape model.

These results provide independent confirmation of the radiometric age estimates and suggest that the evidence for shellfish exploitation documented within the LC-MSA Lower dates to a brief sea level transgression centered at ~167 ka. This brief transgression is also clearly visible in the high-resolution $^{87}Sr/^{86}Sr$ ratio records. Following a peak of 0.70935 at 171.5 ka strontium values rapidly decrease to a low of 0.70925 at 167 ka within a 4.5 ka period before steadily climbing up to the highest radiogenic $^{87}Sr/^{86}Sr$ values of the entire record (0.70967) at 152 ka signaling a major regression at the end of MIS 6. We have argued here and elsewhere (Marean et al., 2007) that these early modern humans focused their settlement on the coast and followed it as it regressed and transgressed through MIS 6. With the LC-MSA Lower deposit we seem to have intercepted the very ephemeral physical signature of this population.

7. Expanding the paleoscape model

Our paleoscape model currently targets the Pinnacle Point area. Correlation of our model to other data, such as strontium isotopes, and evidence for marine resource use at PP13B, supports the local accuracy and relevance of our model in our study area. Guaranteeing the terrestrial (tectonic and geomorphic) and marine (bathymetry) conditions, we suggest that our current paleoscape model can be expanded conservatively along the southern coast of South Africa parallel to the Agulhas Bank using similar methodology.

7.1. Methods

We used bathymetric data derived from satellite altimetry and ship soundings distributed by the GEODESY project[8] to expand our paleoscape model along the South African coast. Unlike our bathymetric data around Pinnacle Point, which was collected using SONAR soundings, GEODESY topography data are derived using ship

[5] The output of the paleoscape model, documenting the distance to the coast during MIS 6 time, was noted in the main text of the paper (Marean et al., 2007) and fully provided in the online Supplementary Information (doi: 10.1038/nature06204).

[6] The minimum and maximum sea level heights described here rely on the 150° route.

[7] However, sea levels between 166 and 169 ka are within the 10 km maximum distance.

[8] http://topex.ucsd.edu/WWW_html/mar_topo.html

Table 1
The average, minimum, and maximum modeled coastlines distances from PP13B in 1.5 ka increments during the LC-MSA. Boundaries for the LC-MSA equate to 2-sigma weighted mean error. This chart also includes the relative sea level heights after Waelbroeck et al. (2002). The results suggest that the coastline would have been within 8 km of Pinnacle Point throughout the entirety of the LC-MSA Upper and much of the LC-MSA Middle. During the LC-MSA Lower, the model results suggests that there was likely only a narrow time period, from 168.5 to 164 ka, when the coast would have been within 8 km of Pinnacle Point.

Age, ka	Average distances		Minimum distances		Maximum distances	
	RSL, meters	Distance, km	RSL, meters	Distance, km	RSL, meters	Distance, km
			No Occupation PP13B			
83.0	−22.30	**0.50**	−9.34	**0.50**	−35.34	**1.68**
84.5	−32.06	**1.68**	−19.11	**0.50**	−45.11	**2.87**
86.0	−41.87	**2.07**	−28.93	**1.27**	−54.93	**7.11**
87.5	−48.63	**4.43**	−34.43	**1.68**	−61.71	**9.13**
89.0	−48.29	**3.73**	−35.37	**1.68**	−61.37	**9.13**
90.5	−47.19	**3.25**	−34.26	**1.68**	−60.26	**8.78**
			Upper Roof Spall/Shelly Brown Sand			
92.0	−42.20	**2.07**	−29.27	**1.27**	−55.27	**7.18**
93.5	−34.74	**1.68**	−21.79	**0.50**	−47.79	**3.63**
95.0	−27.02	**1.27**	−14.07	**0.50**	−40.07	**2.07**
96.5	−27.59	**1.27**	−14.64	**0.50**	−40.64	**2.07**
98.0	−27.81	**1.27**	−14.85	**0.50**	−40.85	**2.07**
			No Occupation PP13B			
99.5	−23.84	**1.06**	−10.87	**0.50**	−36.87	**1.71**
101.0	−20.86	**0.50**	−7.89	**0.08**	−33.89	**1.68**
102.5	−21.18	**0.50**	−8.22	**0.08**	−34.22	**1.68**
104.0	−27.79	**1.27**	−14.83	**0.50**	−40.83	**2.07**
105.5	−31.61	**1.68**	−18.66	**0.50**	−44.66	**2.87**
107.0	−38.03	**1.71**	−25.09	**1.27**	−51.09	**5.23**
108.5	−44.62	**2.87**	−31.69	**1.68**	−57.69	**7.98**
110.0	−44.72	**2.87**	−31.79	**1.68**	−57.79	**7.98**
111.5	−40.94	**2.07**	−28.00	**1.27**	−54.00	**6.80**
113.0	−26.69	**1.27**	−13.74	**0.50**	−39.74	**2.07**
114.5	−17.10	**0.50**	−4.12	**0.08**	−30.12	**1.27**
			LC-MSA Upper			
116.0	−11.42	**0.50**	1.56	**0.08**	−24.44	**1.06**
117.5	−5.45	**0.08**	7.54	**0.08**	−18.46	**0.50**
119.0	−1.16	**0.08**	11.84	**0.08**	−14.16	**0.50**
			LC-MSA Middle			
121.4	2.20	**0.08**	15.20	**0.08**	−10.80	**0.50**
123.9	6.30	**0.08**	19.31	**0.08**	−6.69	**0.08**
126.3	4.91	**0.08**	17.92	**0.08**	−8.08	**0.08**
128.8	−1.25	**0.08**	11.75	**0.08**	−14.66	**0.50**
			LC-MSA Upper			
131.2	−29.39	**1.27**	−16.43	**0.50**	−47.65	**3.63**
132.7	−68.43	**12.51**	−55.54	**7.18**	−81.54	**28.64**
			No Occupation PP13B			
133.8	−84.62	**29.64**	−71.75	**14.53**	−109.87	**68.27**
134.9	−111.46	**70.25**	−98.63	**55.52**	−124.63	**92.71**
135.9	−125.54	**93.48**	−112.73	**72.30**	−138.73	**102.56**
137.0	−128.94	**96.51**	−116.14	**82.46**	−142.14	**103.92**
138.1	−127.05	**94.66**	−114.25	**77.34**	−140.25	**103.27**
139.1	−121.41	**91.91**	−108.60	**67.09**	−134.60	**101.25**
140.2	−117.27	**84.44**	−104.45	**61.18**	−130.45	**97.82**
141.3	−113.29	**73.67**	−92.85	**46.19**	−126.46	**94.28**
142.4	−108.60	**67.09**	−82.57	**29.26**	−121.77	**91.91**
143.4	−105.02	**64.34**	−73.14	**14.69**	−118.18	**86.00**
144.5	−103.84	**60.79**	−71.92	**14.53**	−117.00	**84.41**
146.0	−105.02	**64.34**	−79.46	**25.33**	−118.18	**86.00**
147.5	−113.28	**73.67**	−87.13	**33.98**	−126.45	**94.28**
149.0	−118.79	**87.57**	−92.37	**44.63**	−131.97	**99.24**
150.5	−119.99	**91.11**	−94.96	**50.92**	−133.17	**100.19**
152.0	−118.94	**87.79**	−94.31	**49.74**	−132.12	**99.39**
			LC-MSA Lower			
153.5	−111.98	**71.02**	−89.18	**39.51**	−125.15	**93.09**
155.0	−95.63	**52.10**	−82.78	**29.26**	−108.78	**67.09**
156.5	−76.94	**22.59**	−64.06	**10.34**	−90.06	**41.46**
158.0	−85.45	**30.66**	−71.98	**14.53**	−98.58	**55.52**
159.5	−89.35	**40.03**	−69.17	**12.71**	−102.49	**59.61**
161.0	−79.08	**24.91**	−66.20	**11.14**	−92.20	**44.63**
162.5	−78.58	**24.53**	−65.65	**11.14**	−91.70	**43.83**
164.0	−64.06	**10.34**	−51.16	**5.23**	−77.16	**22.96**
165.5	−51.41	**5.23**	−38.49	**1.71**	−64.49	**10.49**
167.0	−49.53	**4.81**	−36.61	**1.68**	−62.61	**9.16**
168.5	−57.44	**7.76**	−44.53	**2.87**	−70.53	**13.81**
170.0	−66.06	**11.14**	−53.16	**6.41**	−79.16	**25.26**
171.5	−76.51	**22.16**	−63.63	**10.34**	−89.63	**40.70**
173.0	−77.72	**23.35**	−64.84	**10.72**	−90.84	**42.64**
174.5	−72.70	**14.69**	−59.81	**8.48**	−85.81	**30.82**
176.0	−67.91	**11.91**	−55.01	**7.11**	−81.01	**28.64**

soundings and also marine gravity anomalies measured with the ERS-1 and Geosat spacecrafts. Marine gravity anomalies are closely related to oceanic topography within the 15–200 km wavelength. Discussion of the methods and theory to derive seafloor topography from satellite altimetry can be found in Dixon et al. (1983), Smith and Sandwell (1997), and Sandwell and Smith (2000).

We used the GEODESY 1-arc minute topography data to expand our paleoscape model because of data availability along the South African coast. The GEODESY data provide a global, relatively high-resolution, systematic-produced combined topography and bathymetry data set. We find that there is a high correlation between the coastline distances derived using our higher-resolution SONAR data and the GEODESY data around Pinnacle Point; the array of coastline distances derived using each data set share 94.28% of the ranked variation (Spearman rho, $p < .01$). There are some differences between these coastline estimates, however, but the largest errors (>2.5 km) only occur beyond 10 km distance from Pinnacle Point. Therefore, we believe that the GEODESY data are satisfactory for modeling coastline estimates where we do not have the higher-resolution data that we have for Pinnacle Point, but we concede that whenever possible the highest resolution data available should be used.

GEODESY data are provided in 1-arc minute ASCII XYZ coordinate pairs. At mean sea level along the equator, 1-arc minute is approximately 1.86 km (i.e. 1 nautical mile). However, the distance within 1 minute of arc (MOA) varies based upon the radius of the earth at specific latitude. This distance can be calculated using the following formula,

$$d = 2(\Pi r \cos(\theta))/21,600$$

where:

d = distance of 1 MOA at latitude θ
r = radius of the earth at the equator (6378.137 km)
θ = angle of latitude

Our GEODESY data are distributed from 35° 30′ south latitude to 38° south latitude. This means that the point distance within 1 MOA varies from 1.56 km (35° 30′S) to 1.46 km (38° S). To account for this range of distances, we chose to use the averaged 1 MOA distance across our selected data range, which was calculated to 1.51 km. This value was then applied as our raster cell size during the interpolation of the elevation model.

The longitudinal extent of our GEODESY data selection also required the use of a different projection system. The South Africa National Grid uses a Gauss–Krüger projection and subdivides the earth into 2° belts centered on an odd-numbered longitude of origin (Lo.). Distortion is absent along the Lo but it increases outward toward the belt peripheries. Thus if the projected data falls too far beyond the Lo then the distortion may become so extreme that the data will not project back to the same position. Our GEODESY data selection spans 22.75° longitude and it would require 5 Lo belts to project the data properly. To be used properly within a continuous model, these data would need to be subset, projected into the appropriate Lo belt, and then merged back together to create a single elevation model. However, any spatial distortion across the individual Lo belts would be retained in the merged model and, most importantly, the spatial distortion would be distributed unsystematically across the model making it unreliable. Therefore, we chose to project the data instead using the Universal Transverse Mercator (UTM) projection (zone 34S). UTM belts are wider (6°) and because of the 0.996 scaling factor and system of false eastings, there is actually a 500 km buffer to either side of the central meridian where distortion is still minimal (Fenna, 2007:423). Projection and geographic coordinate system parameters for UTM zone 34S are provided in the Supplementary Materials, section 1.2.

We found that ordinary kriging using an exponential semivariogram provided a mean prediction error of 6.07×10^{-4} and a standard deviation of the mean prediction error (RMS) of 30.79. Full model parameter and validation results are provided in the Supplementary Materials, section 2.2. The raster cell size of our final elevation model was 1.51 km, which is based on the averaged distance within 1 MOA across the latitudinal range out our data. This value is also representative of the expected error within our modeling results. Since this value exceeds 0.5 km we believe it can also affect our interpretations of marine resource transportation and we have included the error in the distances modeled below.

7.2. Blombos cave

Blombos cave (BBC) is located ~100 m inland within a wave cut cliff face at an elevation of +35 m (Henshilwood et al., 2001a). The site contains in situ stratified MSA deposits capped by a sterile dune which is overlaid by *in situ* stratified LSA deposits (Henshilwood et al., 2001a,b; Jacobs et al., 2003a,b, 2006).

The MSA deposits are subdivided into three facies: M1, M2, and M3,[9] with a sterile dune capping the sequence. The dune is tightly dated to ~70 ka using OSL (Jacobs et al., 2003a,b). The uppermost M1 deposits are dated by OSL (75.6 ± 3.4 ka) (Henshilwood et al., 2004; Jacobs et al., 2006) and TL dating on burnt lithics (74 ± 5 ka) (Tribolo et al., 2006). The M1 deposits are well known for engraved pigment (Henshilwood et al., 2002) and perforated *Nassarius kraussianus* shells (Henshilwood et al., 2004; d'Errico et al., 2005) recovered during excavations which have implications for the development of modern human behavior. The underlying M2 deposits are dated by OSL to between 84.6 ± 5.8 ka and 76.8 ± 3.1 ka. The M3 deposits are the lowermost of the MSA sequence. One single-grain OSL age taken from the top of the M3 sequence provides a minimum date of 98.9 ± 4.5 ka (Jacobs et al., 2006).

Shellfish collected by people are present in each of the MSA facies at Blombos (Henshilwood et al., 2001b). To date, the published densities of shellfish are: M1 (17.5 kg per m^3), M2 (31.8 kg per m^3) and M3 (68.4 kg per m^3) (Henshilwood et al., 2001b). Rocky shore species *T. sarmaticus* (alikreukal/tuban shell), *Perna perna,* and three species of limpets are the most abundant. Drawing from these analyses, Jacobs et al. (2006) have proposed that occupation of the cave was dependent upon the distance to the coastline. Provided that MSA people gathered from very similar shore environments (e.g. substrate, exposure and slope gradient, see Bustamante et al., 1995) throughout the BBC sequence, changing distances to the shoreline (i.e. the foraging radius) appear to have affected the frequencies of shellfish brought back to the cave during periods when sea levels were already sufficiently high to encourage marine resource use. Using coastline distance data generated from our paleoscape model we can now quantitatively test these observations.

7.3. Discussion

Coastline distances from BBC described below are provided in Table 2 and the full array of distances from BBC is provided in the Supplementary Materials, section 3.2. During late MIS 6 (≥135 ka) the coastline was as much as 130 ± 2 km away from BBC, according to our expanded paleoscape model. By ~133 ka, the coastline

[9] These facies are termed BBC 1, BBC 2, and BBC 3 in Henshilwood et al. (2001b).

Table 2
Modeled coastline distances at Blombos cave. These results accord well with faunal evidence from Blombos Cave that indicates marine resource use and support the conclusions of Jacobs et al., (2006) that shellfish collection was directly related to the distance of the site to the coastline.

Age, ka	Average distances		Minimum distances		Maximum distances	
	RLS, meters	Distance, km	RLS, meters	Distance, km	RLS, meters	Distance, km
			M1 Deposits			
72.50	−67.31	**15.56**	−53.92	**7.65**	−80.41	**43.78**
74.00	−44.38	**7.65**	−31.45	**2.33**	−57.45	**9.42**
75.50	−39.62	**4.10**	−26.68	**2.33**	−52.68	**7.65**
77.00	−36.31	**2.33**	−23.37	**2.33**	−49.37	**7.65**
78.50	−25.43	**2.33**	−12.47	**1.45**	−38.47	**4.10**
			M2 Deposits			
80.00	−19.70	**2.33**	−6.73	**1.45**	−32.73	**2.33**
81.50	−18.67	**2.33**	−5.70	**1.45**	−31.70	**2.33**
83.00	−22.30	**2.33**	−9.34	**1.45**	−35.34	**2.33**
84.50	−32.06	**2.33**	−19.11	**2.33**	−45.11	**7.65**
86.00	−41.87	**4.10**	−28.93	**2.33**	−54.93	**7.65**
87.50	−48.63	**7.65**	−34.43	**2.33**	−61.71	**9.42**
89.00	−48.29	**7.65**	−35.37	**2.33**	−61.37	**9.42**
90.50	−47.19	**7.65**	−34.26	**2.33**	−60.26	**9.42**
92.00	−42.20	**7.65**	−29.27	**2.33**	−55.27	**7.65**
93.50	−34.74	**2.33**	−21.79	**2.33**	−47.79	**7.65**
			M3 Deposits			
95.00	−27.02	**2.33**	−14.07	**1.45**	−40.07	**4.10**
96.50	−27.59	**2.33**	−14.64	**1.45**	−40.64	**4.10**
98.00	−27.81	**2.33**	−14.85	**1.45**	−40.85	**4.10**
99.50	−23.84	**2.33**	−10.87	**1.45**	−36.87	**2.33**
101.00	−20.86	**2.33**	−7.89	**1.45**	−33.89	**2.33**
102.50	−21.18	**2.33**	−8.22	**1.45**	−34.22	**2.33**

began to transgress rapidly and by ~130 ka the coastline was within sufficient distance of BBC to facilitate marine resource collection.

From 104 to 95 ka, which includes the deposition time of the M3 facies at ~100 ka, the average coastline distance was at all times ~2 ± 2 km of BBC. The maximum calculated coastline distances during this time do not exceed 4.1 ± 2 km of BBC. M3 is known to have the highest densities of shellfish at BBC, with more limpets (particularly of the kind with heavier shells) and highest ratio of shell weight to operculum weight for the large turban snail *T. sarmaticus* in the entire sequence. These findings are consistent with the relatively close coastline projected by our model.

Moderate coastline retreat during M1 and M2 is also predicted by the paleoscape model. The average coastline distance predicted during early M2 (~90–78 ka) is ~7.5 ± 2 km distant from the site. After ~85 ka, the coastline becomes unstable and from then until 77 ka, the coastline was within ~2 ± 2 km of BBC. After 77 ka, our model predicts that the coastline regressed slightly, up to ~4 ± 2 km from BBC, and continued to regress into MIS 4. The M1 deposits, which are currently dated 75.6 ± 3.4 ka contain shellfish and Still Bay artifacts. More recent age estimates for the Still Bay argue for a narrower timeframe centered at 71 ka (Jacobs et al., 2008). Within the time range for the M1 deposits, our coastline model suggests that the coast was within range of BBC ≥74 ka. Given the potential divergence between the globally tuned ages and the error on the OSL ages, we still consider these results concordant.

In summary, the paleoscape model accords well with the archaeological evidence from Blombos. The correlation between coastline distance to the coastline and shellfish densities proposed by Jacobs et al. (2006) is also supported for the M1 and M2 facies through our model results. Moreover, our results support another observation made by Henshilwood et al. (2001b:442) that the coastline must have been farther from Blombos during M1 and M2 times because of the markedly higher mussel frequencies during the accumulation of both of these facies than during M3. Mussels have been shown to be transported farther than limpets and other species through both archaeological and ethnographic case studies (they keep better because they are a bivalve) (Meehan, 1982; Parkington et al., 1988). Accordingly, the greater frequencies of shellfish seen in the M3 facies are possibly due to a nearby coastline. A minor regression during M2 times still situated the coastline within 8 km of BBC, but despite a slightly longer overall distance to the coast a longer exposure to the coastline still can account for the frequencies of shellfish seen in these deposits. The M1 deposits, with the least amount of shellfish may be due, in part, to a more limited exposure to the coast only prior to 74 ka.

8. Conclusions

Recently, Bailey and Flemming (2008) have called for a more rigorous approach to studying coastal adaptations and currently coastal landscapes that were, in the past, significantly altered by changing sea levels. We agree. We contend that as part of a more rigorous approach to the study of now-coastal archaeological sites the target should be a paleoscape model that begins with accurate and precise reconstructions of coastline distance and configuration over time at increments useful to understanding ancient human land use.

In the past, researchers have relied on laborious and static approaches to estimate coastline distance and coastline configuration. While our approach requires substantial time investment in the construction of the model, once the model is created then generating output is easy and straightforward. Importantly, the model is dynamic and developments in GIS, computer 3D modeling, and construction of sea level curves allow us to improve dramatically on prior approaches with accurate and precise coastline distance estimates. Our model is also organic in that as age estimates change, bathymetric data improves, and the sea level curves become better resolved, we can quickly improve the model. This framework provides a means to render, view, and analyze our data in a geometric construct more similar to the physical world in which we live, rather than just through tables and static figures. But of equal importance, this framework, the model itself, and also each data source, can be tested, refined, and rejected, if necessary. We thus move beyond purely graphic modeling toward a more engaging, sensible, and modern way to understand our world, past and present (for further, see the Supplementary Video).

Paleoscape modeling may also contribute new understanding of the limitations and possibilities that were likely experienced by humans living astride coastal shelves like the Agulhas Bank during the Middle and Late Pleistocene. Importantly, joining the model to geophysical data could allow us to model soil, sediment, and topography on the Agulhas Bank at specific time slices. Variation in the current Cape Flora is strongly conditioned by rainfall amount, season of rainfall, topography, and soil conditions (Goldblatt and Manning, 2002; Proches et al., 2006; Cowling et al., 2008). If we join our model to reconstructions of rainfall season and amount (Chase and Meadows, 2007; Lewis, 2008), we have the possibility of modeling floral zones on the ancient exposed continental shelf at specific slices through time. This is the next step in our effort.

Here, we have demonstrated our beginning paleoscape model for Pinnacle Point and how it can relate to, and inform upon, other independent approaches. Our example from Blombos cave is only to illustrate the wide-ranging application of this model along the South African coast and, effectively, beyond. At present we have also modeled coastline distances for other important MSA sites from the East and West coasts of South Africa where changes in the continental shelf provide widely varying scenarios. These results will be published in the future as we continue to expand and develop our existing paleoscape model.

Acknowledgements

The authors would like to acknowledge SAHRA and Heritage Western Cape for providing permits to conduct excavations at the aforementioned sites and export of specimens for analysis. We would also like to thank the Mossel Bay community, Mossel Bay municipality, the staff of the Dias museum, and the Cape Nature Conservation.

SACP4 is funded by the National Science Foundation (US) (grants # BCS-9912465, BCS-0130713, and BCS-0524087 to Marean), the Hyde Family Trust, the Institute of Human Origins at Arizona State University, and Arizona State University.

Additionally, we want to thank Dr. Tjeerd H. van Andel and Dr. Charl Bosman for providing bathymetric data around Mossel Bay, Dr. Claire Waelbroeck for providing the reconstructed RSL curve data, and Dr. Richard Wonnacott (Director of Survey Services, Chief Directorate for Surveys and Mapping, South Africa) and Dr. Grenville Barnes (University of Florida) for providing useful geomatic information and suggestions relating to this study. The authors are also very appreciative of the Institute of Social Science Research at ASU for providing facilities and Jong-Geun Kim, also of the ISSR, who developed the sea level slider toolbar plugin for ESRI ArcMap. Finally, we would like to extend our appreciation to the entire MAP and SACP4 research team.

Appendix. Supplementary information

Supplementary information associated with this article can be found, in the online version, at doi:10.1016/j.quascirev.2010.01.015.

References

Ayalon, A., Bar-Matthews, M., Kaufman, A., 1999. Petrography, strontium, barium and uranium concentrations, and strontium and uranium isotope ratios in speleothems as palaeoclimatic proxies: Soreq Cave, Israel. The Holocene 9, 715–722.

Backwell, L., d'Errico, F., 2008. Early hominid bone tools from Drimolen, South Africa. Journal of Archaeological Science 35, 2880–2894.

Bailey, G.N., 2007. Coastlines, submerged landscapes, and human evolution: the Red Sea Basin and the Farasan Islands. The Journal of Island and Coastal Archaeology 2, 127–160.

Bailey, G.N., Craighead, A.S., 2003. Late Pleistocene and Holocene coastal palaeoeconomies: a reconsideration of the molluscan evidence from Northern Spain. Geoarchaeology 18, 175–204.

Bailey, G.N., Flemming, N.C., 2008. Archaeology of the continental shelf: marine resources, submerged landscapes and underwater archaeology. Quaternary Science Reviews 27, 2153–2165.

Banner, J.L., Musgrove, M., Asmerom, Y., Edwards, R.L., Hoff, J.A., 1996. High-resolution temporal record of Holocene ground-water chemistry: tracing links between climate and hydrology. Geology 24, 1049–1053.

Bar-Matthews, M., Marean, C.W., Karkanas, P., Jacobs, Z., Fisher, E., Herries, A.I.R., Ayalon, A., Schilman, B. 2008. A high-resolution and continuous isotopic speloethem record of paleoclimate and paleoenvironment from 92–55 ka from Pinnacle Point, South Africa. The Annual Meeting of the Paleoanthropology Society. Vancouver, British Columbia, March 25–March 26, 2008.

Bar-Matthews, M., Ayalon, A., Kaufman, A., Wasserburg, G.J., 1999. The Eastern Mediterranean paleoclimate as a reflection of regional events: Soreq cave, Israel. Earth and Planetary Science Letters 166, 85–95.

Binford, L.R., 1980. Willow smoke and dogs tails: hunter-gatherer settlement systems and archaeological site formation. American Antiquity 45, 4–20.

Binford, L.R., 1982. The archaeology of place. Journal of Anthropological Archaeology 1, 5–31.

Birch, G.F.D.P.A., Du Plessis, A., Willis, J.P., 1978. Offshore and onland geological and geophysical investigations in the Wilderness Lakes region. Transactions of the Geological Society of South Africa 81, 339–352.

Bird, E.C.F., 2000. Coastal Geomorphology: An Introduction. John Wiley, Chichester.

Bird, D.W., Bliege-Bird, R.L., 1997. Contemporary shellfish gathering strategies among the Meriam of the Torres Strait Islands, Australia: testing predictions of a central place foraging model. Journal of Archaeological Science 24, 39–63.

Bird, D.W., Richardson, J.L., Veth, P.M., Barham, A.J., 2002. Explaining shellfish variability in middens on the Meriam Islands, Torres Strait, Australia. Journal of Archaeological Science 29, 457–469.

Bradley, R.S., 1999. Paleoclimatology: Reconstructing Climates of the Quaternary. Academic Press, San Diego.

Brown, K.S., Marean, C.W., Herries, A.I.R., Jacobs, Z., Tribolo, C., Braun, D., Roberts, D.L., Meyer, M.C., Bernatchez, J., 2009. Fire as an engineering tool of early modern humans. Science 325, 859–862.

Buchanan, W.F., Parkington, J.E., Robey, T.S., and Vogel, J.C., 1984. Shellfish, subsistence and settlement: some western Cape Holocene observations, 121–130.

Bustamante, R.H., Branch, G.M., Eekhout, S., Robertson, B., Zoutendyk, P., Schleyer, M., Dye, A., Hanekom, N., Keats, D., Jurd, M., McQuaid, C.D., 1995. Gradients of intertidal productivity around the coast of South Africa and their relationship with consumer biomass. Oecologia 102, 189–201.

Caputo, R., 2007. Sea-level curves: perplexities of an end-user in morphotectonic applications. Global and Planetary Change 57, 417–423.

Chappell, J., Omura, A., Esat, T., McCulloch, M., Pandolfi, J., Ota, Y., Pillans, B., 1996. Reconciliation of late Quaternary sea levels derived from coral terraces at Huon Peninsula with deep sea oxygen isotope records. Earth and Planetary Science Letters 141, 227–236.

Chappell, J., Shackleton, N.J., 1986. Oxygen isotopes and sea level. Nature 324, 137–140.

Chase, B.M., Meadows, M.E., 2007. Late Quaternary dynamics of southern Africa's winter rainfall zone. Earth Science Reviews 84, 103–138.

Cowling, S.A., Cox, P.M., Jones, C.D., Maslin, M.A., Peros, M., Spall, S.A., 2008. Simulated glacial and interglacial vegetation across Africa: implications for species phylogenies and trans-African migration of plants and animals. Global Change Biology 14, 827–840.

Cowling, R.M., Proches, S., 2005. Patterns and evolution of plant diversity in the Cape Floristic Region. Biologiske Skrifter 55, 273–288.

Deacon, J., Lancaster, N., 1988. Late Quaternary Paleoenvironments of Southern Africa. Clarendon Press, Oxford.

Dixon, T.H., Naraghi, M., McNutt, M.K., Smith, S.M., 1983. Bathymetric prediction from SEASAT Altimiter data. Journal of Geophysical Research-Oceans and Atmospheres 88, 1563–1571.

Ehrlich, S., Gavrieli, I., Dor, L.B., Halicz, L., 2001. Direct high-precision measurements of the Sr-87/Sr-86 isotope ratio in natural water, carbonates and related materials by multiple collector inductively coupled plasma mass spectrometry (MC-ICP-MS). Journal of Analytical Atomic Spectrometry 16, 1389–1392.

Erlandson, J.M., 2001. The archaeology of aquatic adaptations: paradigms for a new millennium. Journal of Archaeological Research 9, 287–350.

d'Errico, F., Henshilwood, C., Vanhaeren, M., van Niekerk, K., 2005. Nassarius kraussianus shell beads from Blombos cave: evidence for symbolic behaviour in the Middle Stone Age. Journal of Human Evolution 48, 3–24.

Fagundes, N.J.R., Ray, N., Beaumont, M., Neuenschwander, S., Salzano, F.M., Bonatto, S.L., Excoffier, L., 2007. Statistical evaluation of alternative models of human evolution. Proceedings of the National Academy of Sciences 104, 17614–17619.

Fenna, D., 2007. Cartographic Science: a Compendium of Map Projections with Derivations. CRC Press, New York.

Flemming, B.W., 1983. Sediment dynamics on the inner Agulhus bank. South African Journal of Science 79, 160–160.

Flemming, B.W., Martin, A.K., Rogers, J., 1983. Onshore and offshore coastal aeolianites between Mossel Bay and Knysna. University of Cape Town Marine Geoscience, Unit Technical Report No. 14, pp. 151–160.

Frumkin, A., Stein, M., 2004. The Sahara-East Mediterranean dust and climate connection revealed by strontium and uranium isotopes in a Jerusalem speleothem. Earth and Planetary Science Letters 217, 451–464.

Goede, A., McCulloch, M., McDermott, F., Hawkesworth, C., 1998. Aeolian contribution to strontium and strontium isotope variations in a Tasmanian speleothem. Chemical Geology 149, 37–50.

Goldblatt, P., 1997. Floristic diversity in the Cape flora of South Africa. Biodiversity and Conservation 6, 359–377.

Goldblatt, P., Manning, J.C., 2002. Plant diversity of the Cape region of southern Africa. Annals of the Missouri Botanical Garden 89, 281–302.

Gonder, M.K., Mortensen, H.M., Reed, F.A., de Sousa, A., Tishkoff, S.A., 2007. Whole-mtDNA genome sequence analysis of ancient African lineages. Molecular Biology and Evolution 24, 757–768.

Grine, F.E., 1998. Additional human fossils from the Middle Stone Age of Die Kelders Cave 1, South Africa:1995 excavation. South African Journal of Science 94, 229–235.

Grün, R., Beaumont, P., Tobias, P.V., Eggins, S., 2003. On the age of Border Cave 5 human mandible. Journal of Human Evolution 45, 155–167.

Haas, J.D., Harrison, G.G., 1977. Nutritional anthropology and biological adaptation. Annual Review of Anthropology 6, 69–101.

Halicz, L., Segal, I., Fruchter, N., Stein, M., Lazar, B., 2008. Strontium stable isotopes fractionate in the soil environments? Earth and Planetary Science Letters 272, 406–411.

Hearty, P.J., Hollin, J.T., Neumann, A.C., O'Leary, M.J., McCulloch, M., 2007. Global sea-level fluctuations during the Last Interglaciation (MIS 5e). Quaternary Science Reviews 26, 2090–2112.

Hendey, Q.B., Volman, T.P., 1986. Last interglacial sea levels and coastal caves in the Cape Province, South Africa. Quaternary Research 2, 189–198.

d'Errico, F., Henshilwood, C.S., 2007. Additional evidence for bone technology in the southern African Middle Stone Age. Journal of Human Evolution 52, 142–163.

Henshilwood, C.S., Nilssen, P., Parkington, J., 1994. Mussel drying and food storage in the late Holocene, SW Cape, South Africa. Journal of Field Archaeology 21, 103–109.

Henshilwood, C.S., D'Errico, F., Marean, C.W., Milo, R.G., Yates, R.J., 2001a. An early bone tool industry from the Middle Stone Age, Blombos Cave, South Africa:

implications for the origins of modern human behaviour, symbolism and language. Journal of Human Evolution 41, 631–678.
Henshilwood, C.S., Sealy, J.C., Yates, R.J., Cruz-Uribe, K., Goldberg, P., Grine, F.E., Klein, R.G., Poggenpoel, C., van Niekerk, K., Watts, I., 2001b. Blombos cave, southern Cape, South Africa: preliminary report on the 1992–1999 excavations of the Middle Stone Age levels. Journal of Archaeological Science 28, 421–448.
Henshilwood, C.S., d'Errico, F., Yates, R., Jacobs, Z., Tribolo, C., Duller, G.A.T., Mercier, N., Sealy, J.C., Valladas, H., Watts, I., Wintle, A.G., 2002. Emergence of modern human behavior: Middle Stone Age engravings from South Africa. Science 295, 1278–1280.
Henshilwood, C., d'Errico, F., Vanhaeren, M., van Niekerk, K., Jacobs, Z., 2004. Middle Stone Age shell beads from South Africa. Science 304, 404.
Imbrie, J., Hays, J.D., Martinson, D.G., McIntyre, A., Mix, A.C., Morley, J.J., Pisias, N.G., Prell, W.L., Shackleton, N.J., 1984. The orbital theory of Pleistocene climate:- support from a revised chronology of the marine $\delta^{18}O$ record. In: Palisades, N.Y., Berger, A., Imbrie, J., Hays, H., Kukla, G., Saltzman, B. (Eds.), Milankovitch and Climate: Understanding the Response to Astronomical Forcing. Proceedings of the NATO Advanced Research Workshop Held 30 November–4 December, 1982. D. Reidel Publishing, Dordrecht.
Ingman, M., Kaessmann, H., Paabo, S., Gyllensten, U., 2000. Mitochondrial genome variation and the origin of modern humans. Nature 408, 708–713.
Jacobs, Z. An OSL chronology for the sedimentary deposits from Pinnacle Point Cave 13B – a punctuated presence. Journal of Human Evolution, submitted for publication.
Jacobs, Z., Duller, G.A.T., Wintle, A.G., 2003a. Optical dating of dune sand from Blombos Cave, South Africa: II–single grain data. Journal of Human Evolution 44, 613–625.
Jacobs, Z., Wintle, A.G., Duller, G.A.T., 2003b. Optical dating of dune sand from Blombos Cave, South Africa: I–multiple grain data. Journal of Human Evolution 44, 599–612.
Jacobs, Z., Duller, G.A.T., Wintle, A.G., Henshilwood, C.S., 2006. Extending the chronology of deposits at Blombos Cave, South Africa, back to 140 ka using optical dating of single and multiple grains of quartz. Journal of Human Evolution 51, 255–273.
Jacobs, Z., Roberts, R.G., Galbraith, R.F., Deacon, H.J., Grun, R., Mackay, A., Mitchell, P., Vogelsang, R., Wadley, L., 2008. Ages for the Middle Stone Age of Southern Africa: implications for human behavior and dispersal. Science 322, 733–735.
Jacobs, Z., Roberts, R.G., 2007. Advances in optically stimulated luminescence dating of individual grains of quartz from archaeological deposits. Evolutionary Anthropology 16, 210–223.
Jerardino, A., 2003. Pre-colonial settlement and subsistence along sandy shores south of Elands Bay, West Coast, South Africa. South African Archaeological Bulletin 58, 53–62.
Jerardino, A., Marean, C.W. Shellfish gathering, marine palaeoecology and modern human behavior: perspectives from cave PP13b, Pinnacle Point, South Africa. Journal of human evolution, in press.
Jouzel, J., Hoffmann, G., Parrenin, F., Waelbroeck, C., 2002. Atmospheric oxygen 18 and sea-level changes. Quaternary Science Reviews 21, 307–314.
Kelly, R.L., 1983. Hunter-gatherer mobility strategies. Journal of Anthropological Research 39, 277–306.
Kelly, R.L., 1995. The Foraging Spectrum. Smithsonian Institution Press, Washington, DC.
Klein, R.G., 1972. The late quaternary mammalian fauna of Nelson Bay Cave (Cape Province, South Africa): its implications for megafaunal extinctions and environmental and cultural change. Quaternary Research 2, 135–142.
Klein, R.G., 1976. The mammalian fauna of the Klasies River mouth sites, southern Cape Province, South Africa. South African Archaeological Bulletin 31, 75–98.
Klein, R.G., Deacon, H.J., Hendey, Q.B., Lambrechts, J.J.N., 1983. Palaeoenvironmental implications of Quaternary large mammals in the fynbos region. In: Deacon, H.J., Hendey, Q.B., Lambrechts, J.J.N. (Eds.), Fynbos Palaeoecology: a Preliminary Synthesis. South African National Scientific Programmes, CSIR, pp. 116–138. SANSP Report 75.
Lambeck, K., Esat, T.M., Potter, E.K., 2002. Links between climate and sea levels for the past three million years. Nature 419, 199–206.
Lee, R.B., 1972. Kung spatial organization: an ecological and historical perspective. Human Ecology 1, 73–97.
Lee, R.B., Lee, R.B., DeVore, I., 1968. What hunters do for a living, or, how to make out on scarce resources. In: Lee, R.B., DeVore, I. (Eds.), Man the Hunter. Aldine, Chicago, pp. 30–48.
Lewis, C.A., 2008. Late Quaternary climatic changes, and associated human responses, during the last ~45,000 yr in the Eastern and adjoining Western Cape, South Africa. Earth Science Reviews 88, 167–187.
Mackay, A., Welz, A., 2008. Engraved ochre from a Middle Stone Age context at Klein Kliphuis in the Western Cape of South Africa. Journal of Archaeological Science 35, 1521–1532.
Malan, J.A., 1987. The Bredasdorp group in the area between Gans Bay and Mossel Bay. South African Journal of Science 83, 506–507.
Malan, J.A., 1991. Lithostratigraphy of the Klein Brak formation (Bredarsdorp group). In: South African Committee for Stratigraphy: Lithostratigraphic Series. Department of Mineral and Energy Affairs, Geological Survey, pp. 1–13.
Marean, C.W., 2000. The Middle Stone Age at Die Kelders Cave 1, South Africa. Journal of Human Evolution 38, 3–5.
Marean, C.W., Assefa, Z., 2005. The middle and upper Pleistocene African record for the biological and behavioral origins of modern humans. In: Stahl, A. (Ed.), African Archaeology: a Critical Introduction. Blackwell Publishing Ltd, New York, pp. 93–129.
Marean, C.W., Nilssen, P.J., Brown, K., Jerardino, A., Stynder, D., 2004. Paleoanthropological investigations of Middle Stone Age sites at Pinnacle point, Mossel Bay (South Africa): archaeology and hominid remains from the 2000 field season. Paleoanthropology 2, 14–83.
Marean, C.W., Bar-Matthews, M., Bernatchez, J., Fisher, E., Goldberg, P., Herries, A.I.R., Jacobs, Z., Jerardino, A., Karkanas, P., Minichillo, T., Nilssen, P.J., Thompson, E., Watts, I., Williams, H.M., 2007. Early human use of marine resources and pigment in South Africa during the Middle Pleistocene. Nature 449, 905–908.
Marean, C.W., Bar-Matthews, M., Fisher, E.C., Goldberg, P., Herries, A., Karkanas, P., Nilssen, P., Thompson, E.. The stratigraphy of the Middle Stone Age sediments at Pinnacle Point Cave 13B (Mossel Bay, western Cape Province, South Africa). Journal of Human Evolution, in press.
Marker, M.E., 1984. Marine benches of the Eastern Cape, South Africa. Transactions of the Geological Society of South Africa 87, 11–18.
Marker, M.E., 1987. A note on marine benches of the southern Cape. South African Journal of Geology 90, 120–123.
Martinson, D.G., Pisias, N., Hays, J.D., Imbrie, J., Moore Jr., T.C., Shackleton, N.J., 1987. Age dating and the orbital theory of the ice ages: development of a high-resolution 0–300,000-year chronostratigraphy. Quaternary Research 27, 1–29.
McBrearty, S., Brooks, A.S., 2000. The revolution that wasn't: a new interpretation of the origin of modern human behavior. Journal of Human Evolution 39, 453–563.
McDougall, I., Brown, F.H., Fleagle, J.G., 2005. Stratigraphic placement and age of modern humans from Kibish, Ethiopia. Nature 433, 733–736.
Meehan, B., 1982. Shell Bed to Shell Midden. Australian Institute of Aborginal Studies, Atlantic Highlands.
Musgrove, M., Banner, J.L., 2004. Controls on the spatial and temporal variability of vadose dripwater geochemistry: Edwards aquifer, central Texas. Geochimica et Cosmochimica Acta 68, 1007–1020.
Olson, S.L., Hearty, P.J., 2009. A sustained +21 m sea-level highstand during MIS 11 (400 ka): direct fossil and sedimentary evidence from Bermuda. Quaternary Science Reviews 28, 271–285.
Parkington, J., Poggenpoel, C., Buchanan, W., Robey, T., Manhire, T., Sealy, J., Bailey, G., Parkington, J., 1988. Holocene coastal settlement patterns in the Western Cape. In: Bailey, G., Parkington, J. (Eds.), The Archaeology of Prehistoric Coastlines. Cambridge Univ. Press, NY, pp. 22–41.
Proches, S., Cowling, R.M., Goldblatt, P., Manning, J.C., Snijman, D.A., 2006. An overview of the Cape geophytes. Biological Journal of the Linnean Society 87, 27–43.
Ramsay, P.J., Cooper, J.A., 2002. Late Quaternary sea-level change in South Africa. Quaternary Research 57, 82–90.
Rightmire, G.P., Deacon, H.J., Schwartz, J.H., Tattersall, I., 2006. Human foot bones from Klasies River main site, South Africa. Journal of Human Evolution 50, 96–103.
Sandwell, D.T., Smith, W.H.F., 2000. Bathymetric estimation. In: Fu, L.-L., Cazenave, A., Holton, G.A. (Eds.), Satellite Altimetry and Earth Sciences: a Handbook of Techniques and Applications. International Geophysics Series. Academic Press, San Diego, pp. 441–456.
Shackleton, N.J., 1987. Oxygen isotopes, ice volume and sea level. Quaternary Science Reviews 6, 183–190.
Shackleton, N.J., Opdyke, N.D., 1973. Oxygen isotope and palaeomagnetic stratigraphy of equatorial pacific core V28–238: oxygen isotope temperatures and ice volumes on a 10/5 year and 10/6 year scale. Quaternary Research 3, 39–55.
Silberbauer, G.B., 1981. Hunter and Habitat in the Central Kalahari Desert. Cambridge University Press, Cambridge.
Smith, W.H.F., Sandwell, D.T., 1997. Global sea floor topography from satellite altimetry and ship depth soundings. Science 277, 1956–1962.
Tanaka, J., 1980. The San Hunter-Gatherers of the Kalahari: a Study in Ecological Anthropology. University of Tokyo Press, Tokyo.
Tribolo, C., Mercier, N., Selo, M., Valladas, H., Joron, J.L., Reyss, J.L., Henshilwood, C., Sealy, J., Yates, R., 2006. TL dating of burnt lithics from Blombos Cave (South Africa): further evidence for the antiquity of modern human behaviour. Archaeometry 48, 341–357.
Tribolo, C., Mercier, N., Valladas, H., Joron, J.L., Guibert, P., Lefrais, Y., Selo, M., Texier, P.J., Rigaud, J.P., Porraz, G., Poggenpoel, C., Parkington, J., Texier, J.P., Lenoble, A., 2009. Thermoluminescence dating of a Stillbay-Howiesons Poort sequence at Diepkloof Rock Shelter (Western Cape, South Africa). Journal of Archaeological Science 36, 730–739.
USGS, 2004. Shuttle Radar Topography Mission, 3 Arc Seconds Scene SRTM_u03_p172r084, Unfilled Unfinished 2.0. In: Global Land Cover Change Facility. University of Maryland, College Park, Maryland.
Van Andel, T.H., 1989. Late Pleistocene sea levels and the human exploitation of the shore and shelf of southern south Africa. Journal of Field Archaeology 16, 133–155.
Verhyden, S., Keppens, E., Fairchild, I.J., McDermott, F., Weis, D., 2000. Mg, Sr and Sr isotope geochemistry of Belgian Holocene speleothems: implications for paleoclimate reconstructions. Chemical Geology 169, 131–144.
Vogel, J.C., Tobias, P.V., Raath, M.A., Maggi-Cecchi, J., Doyle, G.A., 2001. Radiometric dates for the Middle Stone age in South Africa. In: Tobias, P.V., Raath, M.A., Maggi-Cecchi, J., Doyle, G.A. (Eds.), Humanity from African Naissance to Coming Millennia. Florence University Press, Florence, pp. 261–268.
Waelbroeck, C., Labeyrie, L., Michel, E., Duplessy, J.C., McManus, J.F., Lambeck, K., Balbon, E., Labracherie, M., 2002. Sea-level and deep water temperature

changes derived from benthic foraminifera isotopic records. Quaternary Science Reviews 21, 295–305.
Watts, I., 2002. Ochre in the Middle Stone Age of southern Africa: ritualized display or hide preservative? South African Archaeological Bulletin 57, 1–14.
Watts, I., Dunbar, R., Knight, C., Power, C., 1999. The origin of symbolic culture. In: Dunbar, R., Knight, C., Power, C. (Eds.), The Evolution of Culture. Edinburgh University Press, Edinburgh, pp. 113–146.
White, T.D., Asfaw, B., DeGusta, D., Gilbert, H., Richards, G.D., Suwa, G., Howell, F.C., 2003. Pleistocene Homo sapiens from middle Awash, Ethiopia. Nature 423, 742–747.
de Wit, M., 2007. The Kalahari epeirogeny and climate change: differentiating cause and effect from core to space. South African Journal of Geology 110, 367–392.
Woodroffe, C.D., 2003. Coasts: Form, Process, and Evolution. Cambridge University Press, New York.